THE INFLUENCE OF TEMPERATURE AND PREFERRED ORIENTATION ON HALL COEFFICIENT AND RESISTIVITY OF PURE TITANIUM

LOUIS C. ROESCH

NOVEMBER 1962

A REPORT ON RESEARCH CONDUCTED FOR THE U.S. AIR FORCE OFFICE OF SCIENTIFIC RESEARCH UNDER CONTRACT NO. 49(638)-1034

W. M. KECK LABORATORY OF
ENGINEERING MATERIALS

CALIFORNIA INSTITUTE OF TECHNOLOGY

PASADENA

CALIFORNIA INSTITUTE OF TECHNOLOGY

W. M. KECK LABORATORY OF ENGINEERING MATERIALS

THE INFLUENCE OF TEMPERATURE AND PREFERRED ORIENTATION ON HALL COEFFICIENT AND RESISTIVITY OF PURE TITANIUM

Louis C. Roesch

Technical Report to

Solid State Sciences Division, Air Force Office of

Scientific Research, Washington 25, D. C.

November 1962

Approved by Pol Duwez
Professor of Engineering
Principal Investigator Contract No. 49(638)-1034
Division File No. 50-5

TABLE OF CONTENTS

ACKNOWLEDGEMENTS

The writer wishes to express his deep gratitude to Professor Pol Duwez for his encouragement and advice during the course of this investigation. The author also wishes to thank Dr. R. H. Willens for his assistance, advice and numerous helpful suggestions, which greatly facilitated this study. He also acknowledges the assistance of Messrs. M. Krone and F. Youngkin for their assistance in the construction of the apparatus and in the performance of some of the experiments. Thanks are due to Miss L. Bartley, who typed the manuscript and to Mr. R. Bloom who prepared most of the tracings.

ABSTRACT

An experimental apparatus capable of measuring voltages in the microvolt region with an accuracy of $\pm 5.10^{-9}$ volts is used to determine the temperature variation of resistivity and Hall coefficient of three specimens of iodide titanium. These specimens are of comparable purity (room temperature to liquid helium temperature resistance ratio near 30) and possess a high degree of preferred orientation. The measurements are made at temperatures between 4.2 and 300°K.

The Hall coefficient is found to depend strongly on temperature and crystalline texture. At room temperature it has a value of -1.8×10^{-11} m^3/coulomb in two specimens, whereas in the third it equals $+ 1.2.10^{-11}$ m^3/coulomb. Several factors including impurities, changes in the scattering mechanism, size effects, crystallographic anisotropy, which could account for the observed differences, are discussed and it is proposed that crystallographic orientation is the most influential factor. From the measured data and a phenomenological theory of the Hall effect developed in the case of single crystals, values of the components of the galvanomagnetic tensor, which replaces the scalar Hall coefficient of isotropic media, are calculated and discussed in connection with a possible model of the Fermi surface of titanium.

Only tentative conclusions can be drawn from the present experimental investigation and no definite explanation can be offered for the difference in the signs of the two principal galvanomagnetic coefficients. Additional measurements on single crystals and extension of these measurements to higher temperatures, as well as intestigations of other properties of titanium (topological measurements in particular) must be made before a more comprehensive band model of titanium metal can be established.

1. INTRODUCTION

The possibility of an effect of a magnetic field on the process of electrical conduction was first suggested by W. Thomson in 1851 when he noticed a variation in thermoelectric power of magnetized iron when the orientation of the magnetic field was changed. In 1858 the discovery of an increase in resistivity in the presence of a magnetic field opened the field of galvanomagnetic and thermomagnetic effects. However, no transverse effect was discovered until 1879 when E. H. Hall measured a transverse electric field in thin gold plates[1]. In 1883 A. Righi found a similar effect in bismuth but a thousand times stronger than in gold. Since then the Hall effect has been measured in many materials, especially metals, and theories have been proposed to explain it in the light of the electron theories of transport properties. The interpretation of experimental measurements led to quantitative determination of certain important parameters of these theories.

In the Hall effect a current carrying conductor is placed in a transverse magnetic field. An electric field, called the Hall field, appears in a direction perpendicular to both the magnetic field and the current flow. In many cases this field is proportional to the magnetic field strength and the current density. The proportionality constant or Hall coefficient combined with the electrical conductivity yields information which is useful in determining the densities, mobilities and exact nature (electrons or holes) of the charge carriers responsible for electrical conduction. Metallic conduction is characterized by a small Hall coefficient which changes little with temperature and a resistivity

which increases with temperature. In order to explain the sign, magnitude, temperature and magnetic field dependences, a detailed band model for the conductor has to be used.

Since the Hall effect allows estimates to be made of the number of conducting particles per unit volume and their sign, this measurement is expected to be helpful in the determination of the rather complicated band structure of the transition elements. In these metals both electrons and holes contribute to conduction and thus no quantitative information can be obtained from Hall effect and resistivity alone. Their temperature dependence can lead to further information on the electronic structure. In particular, the question of how many of the outer electrons are actually "free", i.e., are responsible for the metallic properties of these elements, might be clarified. The Hall coefficient has been measured at room temperature for the elements of the first transition period[2]: it is positive and large for chromium, positive and intermediate for vanadium and manganese, positive and small for iron, rather small but negative for cobalt and nickel (Fig. 1). For titanium it is small but its sign is not established with certainty.

The present investigation was undertaken in the hope of finding an explanation for the contradictory data on Hall effect published for titanium. Besides the uncertainty in the sign of the Hall coefficient, its variation with temperature could not be characterized by a single curve (Fig. 2). G. Scovil[3] reported first a positive value of the Hall coefficient: $R = (2.8 \pm 0.9) \times 10^{-11}$ m^3/coulomb at about 100°C.

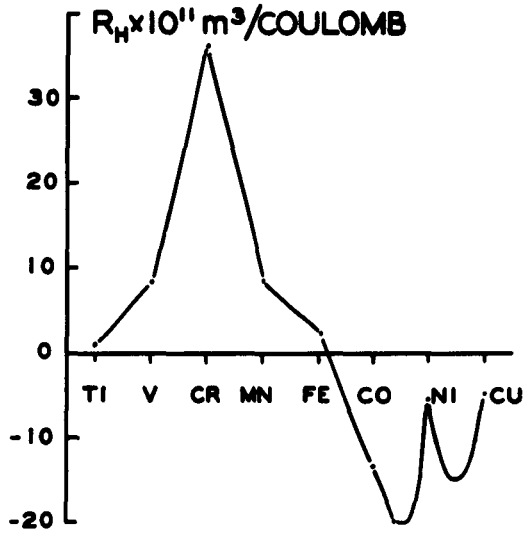

Fig. 1. Hall coefficient of various 3d transition elements at room temperature.

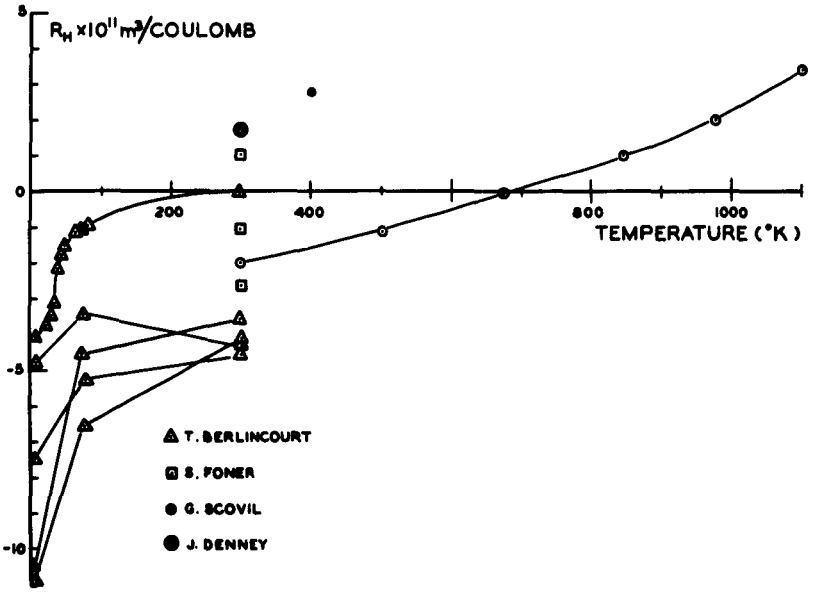

Fig. 2. Hall coefficient of titanium as a function of temperature.

This value was explained by an overlapping of the energy bands and a predominant contribution from holes. In a later series of measurements[4] over a temperature range from 300 to 1100°K, the Hall coefficient was found to reverse its sign from negative to positive at 675 ± 30°K. Just above room temperature its value is -2.0×10^{-11} m^3/coulomb: it increases smoothly with temperature and equals $+3.5 \times 10^{-11}$ m^3/coulomb at 1100°K. This behavior was attributed to anisotropic thermal expansion causing a change in the shape and mobilities in the 3d band. The relative proportion of electrons and holes may vary, causing the Fermi level to shift such as to decrease the density of holes and thus increase their mobility. As temperature increases the contribution of holes becomes predominant. This interpretation accounts also for the temperature dependence of the electrical resistivity.

S. Foner[2] studied three sheet specimens at room temperature. In the three cases the Hall voltage was found to be rigorously proportional to the applied field but the Hall coefficients were different:

Specimen	Treatment	Hall coefficient
I	as machined	-1.06×10^{-11}
II	annealed for 2 hours at 600°C	-2.59×10^{-11} m^3/Cb
III	annealed for 6 hours at 800°C	$+1.02 \times 10^{-11}$

The differences between the three specimens were attributed to impurities and differences in the preparation of the samples. The small magnitude was thought to be due to the balancing effect of holes and electrons in the overlapping 3d, 4s and 4p bands. Negative values were correlated with commercial grade titanium[5].

More recent data are provided by the work of T. G. Berlincourt[6]. Five samples were studied between 1°K and room temperature. The Hall voltage was a linear function of magnetic field strength at all temperatures. However, the data revealed a great sensitivity of the Hall coefficient to impurity content. It was also suggested that preferred orientation contributed to the broad spectrum of observed values. The temperature dependence of the Hall constant was weak in the residual and linear resistivity temperature regions and strong near 30°K.

The purpose of the present study was to investigate the influence of preferred orientation on the Hall effect and possibly to detect any crystallographic anisotropy which could account for the scattering in the experimental observations.

2. FORMULATION AND MEASUREMENT OF THE HALL EFFECT

2.1 Definitions and Notations

Consider a conductor having the shape of a rectangular parallelepiped and a cartesian system of coordinates the axes of which are parallel to the edges of the specimen (in practice a long thin plate). A current of uniform density J flows in the x direction and a magnetic field of intensity H is applied parallel to the z axis (Fig. 3a). An electric field E_H appears then in the y direction.

2.11 The Hall coefficient

In most instances the Hall field E_H is proportional to the current density J and the magnetic induction B, which for most practical cases is numerically equal to the applied field H. The phenomenon can therefore be characterized by the value of the proportionality constant R_H:

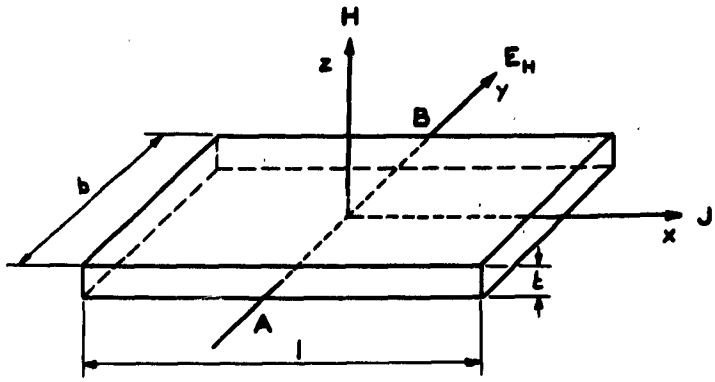

a

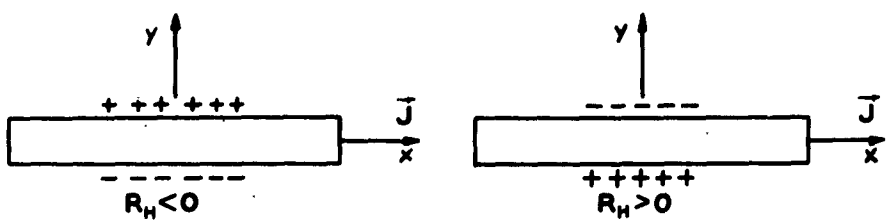

H IS NORMAL TO THE DRAWING AND POINTS TOWARD THE READER

b

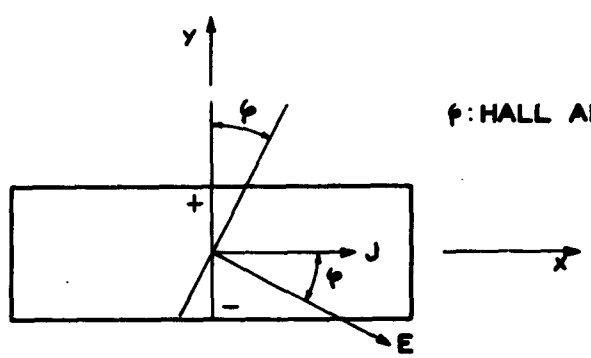

c

Fig. 3. a. Geometry of a Hall measurement specimen
b. Sign of the Hall coefficient
c. Hall angle

$$E_H = R_H JB$$

In practice one measures the transverse voltage between A and B and the total current I through the sample. Then the Hall coefficient R_H is defined by:

$$R_H = \frac{t}{BI} V_H$$

since $I = btJ$ and $V_H = bE_H$; b is the dimension of the sample in the y direction, t its thickness in the z direction; R_H is characteristic of the material and usually a function of temperature only. It is commonly expressed in the two following units:

-in practical units t is expressed in cm, B in gauss, I in amperes and V_H in volts. Then R_H is in volt-centimeter per ampere-gauss.

-in the MKS system t is given in meters, B in weber per square meters, I in amperes (absolute), V_H in volts. Then R_H is expressed in cubic meter per coulomb (m^3/Cb).

$$1\ m^3/Cb = 100\ \frac{V\ cm}{amp.\ gauss}$$

The sign of the Hall coefficient is defined in Fig. 3b. For identical carriers a free electron model gives for the Hall coefficient[7]

$$R_H = \frac{1}{Nec}$$

in which N is the carrier concentration, e the carriers' charge and c the velocity of light. If electrons are mostly responsible for the

electrical properties, R_H will be negative. It is positive if holes are predominant.

2.12 Other quantities related to the Hall effect

The Hall effect can also be described as a shift due to the magnetic field of the equipotential surfaces in the conductor. In the absence of the magnetic field, in an isotropic medium, these surfaces are planes normal to the x axis along which the current is flowing. When the magnetic field is applied, electric vector and current density are no longer collinear. In first approximation, neglecting the change in resistivity, this fact is expressed by writing

$$\vec{E} = \rho(0)\,\vec{J} + R_H\,\vec{B} \times \vec{J}$$

In the absence of the magnetic field only the first term is present. A measure of the Hall effect is then the angle φ which exists between the electric field and the current lines (Fig. 3c). This angle is defined and expressed in terms of R_H by the following relation:

$$\tan\varphi = \frac{E_y}{E_x} = \frac{R_H B}{\rho} = \mu B$$

On a single band model μ is the mobility of the charge carriers and is called the Hall angle. It is sometimes useful to use a Hall resistivity or conductivity by expressing J in terms of E.

$$J_x = J = \sigma E_x + \sigma_H E_y$$

where σ is the ordinary conductivity, and σ_H the Hall conductivity. The Hall resistivity can be defined by $E_y = \rho_H J_x$. One frequently

employs the Hall mobility μ_H defined by

$$\mu_H = c\,\sigma\,R_H \qquad \sigma \text{ is the ordinary conductivity.}$$

In the following sections only the Hall coefficient R_H will be considered.

2.2 Anisotropic Hall effect

Experimental investigations of the Hall effect, especially in single crystals, have shown that R_H is not always independent of magnetic induction. Furthermore most materials are not isotropic. Therefore a more general formulation of the Hall effect has to be developed. Scalar quantities like ρ and R_H have to be replaced by tensors. In the remainder of this section we consider only the case of single crystals for which a phenomenological theory of the Hall effect has been obtained.

2.21 Galvanomagnetic coefficients

Consider a rectangular plate cut from a single crystal of a conductor. Two systems of coordinates can be attached to it. The experiment gives quantities in the xyz system whose axes are parallel to the edges of the specimen. Intrinsic properties of the material are better described in the system of coordinates $x_1x_2x_3$ constituted by the conventional principal crystallographic axes associated with the symmetry elements of the crystal. A method is now presented which allows the intrinsic characteristics of the Hall effect to be obtained from quantities measured in the xyz system.

Most generally, the Hall effect has been described as a change in the relationship between the electric field and the current density under the influence of an applied magnetic field. In the absence of any thermal

gradients, even in zero magnetic field, these two vectors are not collinear in the case of anisotropic media. The components of the electric vector are given by:

$$E_i = \rho_{ik} J_k \qquad i = 1,2,3 \qquad k = 1,2,3 \qquad (1)$$

where a summation over k is implied (Einstein's summation convention). ρ_{ik} is the resistivity tensor. This relation takes the same form in any system of coordinates. The components ρ_{ik}, however, differ from one system to another. For the sake of clarity we assume that unless otherwise specified, all equations are written in the $x_1 x_2 x_3$ system.

If an external magnetic field is then applied, equation 1 is still satisfied, but the components of the resistivity tensor become functions of the magnetic induction. For small magnetic fields each component $\rho_{ik}(B)$ can be expanded in a power series[8,9]

$$\rho_{ik}(B) = \rho_{ik} + R_{ik\ell} B_\ell + R_{ik\ell m} B_\ell B_m + \ldots \qquad (2)$$

$i,k,\ell,m\ldots$ take independently the values 1, 2 and 3. $R_{ik\ell}$, $R_{ik\ell m}\ldots$ are called galvanomagnetic coefficients. Most of the observations can be accounted for by keeping only the first two terms of the expansion:

$$E_i = \rho_{ik} J_k + R_{ik\ell} J_k B_\ell \qquad (3)$$

In equation 3 ρ_{ik} stands for $\rho_{ik}(0)$, the resistivity in zero magnetic field. In this form the Hall effect is proportional to both current and magnetic induction. If this is not verified by experiment, higher order terms have to be kept in the expansion. In this form, however, Hall effect and magnetoresistance are not distinguished. In order to separate

them, one has to divide $\rho_{ik}(B)$ into its symmetric and antisymmetric parts

$$\rho_{ik} = s_{ik}(B) + a_{ik}(B)$$

where $s_{ik}(B) = s_{ki}(B) = \frac{1}{2}(\rho_{ik} + \rho_{ki}) = s_{ik}(-B)$ and $a_{ik}(B) = -a_{ki}(B) = \frac{1}{2}(\rho_{ik} - \rho_{ki}) = -a_{ik}(-B)$. The parity and symmetry characters follow from Onsager's reciprocal relations. With these definitions,

$$E_i = s_{ik}J_k + a_{ik}J_k \qquad (4)$$

$a_{ik}J_k$ is a generalization of the Hall field and reverses its sign with B. $s_{ik}J_k$ is the ordinary electric vector modified to take magnetoresistance into account. It is even in B. The Hall effect is then the antisymmetrical part of $\rho_{ik}(B)$ or the fraction of $\rho_{ik}(B)$ which changes its sign when reversing B. The non zero components of $a_{ik}(B)$ can be denoted $R_1 = a_{23}$, $R_2 = a_{31}$, $R_3 = a_{12}$. Then equation 4 becomes

$$E_i = s_{ik}(B)\, J_k + (\vec{J} \times \vec{R})_i \qquad (5)$$

$\vec{R}$ is the vector of components R_i and is designated as the Hall vector. This formulation is physically more significant and can be used to define more meaningful galvanomagnetic coefficients.

T. Okada[10] rewrites equation 5 in an equivalent form, with a slightly different notation.

$$E_i = \rho_{ij}(B)\, J_j + \varepsilon_{ijk}\, J_j R_k(B) \qquad (6)$$

$\rho_{ij}(B)$ is the magnetoresistance tensor (resistivity tensor modified to take the change in resistivity with magnetic field into account). $R_k(B)$ are the components of the Hall vector ($k = 1,2,3$), ε_{ijk} is the Kronecker

antisymmetric symbol and equals 1 if ijk is 123, 231, or 312, -1 if ijk equals 321, 213 or 132 and 0 otherwise.

For small magnetic inductions, $\rho_{ij}(B)$ and $R_k(B)$ can be approximated by power series

$$\begin{aligned} \rho_{ij}(B) &= \rho_{ij}(0) + \rho_{ij.mn} B_m B_n + \cdots \\ R_k(B) &= R_{k.m} B_m + R_{k.mno} B_m B_n B_o + \cdots \end{aligned} \tag{7}$$

If we keep only first order terms, the electric field components become:

$$E_i = \rho_{ij}(0)\, J_j + R_{k.m} B_m J_j\, \varepsilon_{ijk} \tag{8}$$

which is equivalent to equation 3 if we replace $\varepsilon_{ijk} J_j R_{k.m}$ by R_{ijm}. In both cases magnetoresistance effects are completely ignored. The tensor quantities introduced as coefficients in the power series 7 will also be referred to as galvanomagnetic coefficients. In the first order the Hall effect can be described by the second rank tensor $R_{k.m}$, which has nine components. If the Hall field is not proportional to B, higher order galvanomagnetic coefficients like $R_{k.mno}$ can no longer be neglected. The number of independent components of the galvanomagnetic tensors depends on the macroscopic or point-group symmetry of the crystal. In cubic crystals $R_{k.m}$ has only one independent component. The Hall effect is therefore isotropic in these crystals if it is proportional to B. This is no longer true if higher order tensors have to be introduced because they are not isotropic. The effect is always anisotropic for non cubic crystals because $R_{k.m}$ already has less symmetry. Consider now a case where equation 8 can be used. It can be written

$$E_i = E_{Pi} + E_{Hi}$$

where E_p is the primary electric field assumed unaltered by the magnetic field: $E_{Pi} = \rho_{ij}(0)\, J_j$ is Ohm's law; E_H is the Hall field. It changes sign when B is reversed.

The advantage of the tensorial formulation is that relations between physical quantities take the same form in any system of coordinates. One of the equations contained in 8 gives an expression of E_{Hy} in the xyz system

$$E_{Hy} = (R_{x.x}J_z - R_{z.x}J_x)B_x + (R_{x.y}J_z - R_{z.y}J_x)B_y + (R_{x.z}J_z - R_{z.z}J_x)B_z \qquad (9)$$

This is the component which appears between A and B (Fig. 3a). In an actual experiment $J_y = J_z = 0$ and $B_x = B_y = 0$. Then equation 9 reduces to

$$E_{Hy} = -R_{z.z}J_xB_z \qquad (10)$$

From equations 8 and 10

$$E_{Hy} = E_y(B) - E_y(0) = -R_{z.z}J_xB_z \qquad (11)$$

This equation shows how the experiment can lead to a value for $R_{z.z}$ which plays the role of $-R_H$ introduced in section 2.11. With the same assumptions the other components of the Hall field are

$$E_{Hx} = B_z(R_{z.z}J_y - R_{y.z}J_z) = 0$$

$$E_{Hz} = B_z(R_{y.z}J_x - R_{x.z}J_y) = R_{y.z}J_xB_z$$

Using the laws of transformation of tensors with rotation of the coordinate system we can express $R_{z.z}$ in terms of the "intrinsic" galvanomagnetic

coefficients $R_{1.1}$, $R_{1.2}$, etc... (which are nothing but the components of the tensor $R_{k.m}$ in a preferred system of coordinates, namely, the principal axes $x_1x_2x_3$). The change of coordinate system can be written by means of a 3 x 3 unitary matrix:

$$\begin{pmatrix} A_x \\ A_y \\ A_z \end{pmatrix} = \begin{pmatrix} \ell_1 & m_1 & n_1 \\ \ell_2 & m_2 & n_2 \\ \ell_3 & m_3 & n_3 \end{pmatrix} \begin{pmatrix} A_1 \\ A_2 \\ A_3 \end{pmatrix}$$

$\vec{A}$ is a vector of components A_x A_y A_z in the xyz system and A_1 A_2 A_3 in the $x_1x_2x_3$ system. $\ell_1 m_1 n_1$ are the direction cosines of the x axis in the $x_1x_2x_3$ system. J, which is directed along this axis, has then as components in the system of the crystallographic axes:

$$J_1 = \ell_1 J_x \qquad J_2 = m_1 J_x \qquad J_3 = n_1 J_x$$

In this system the components of the Hall field are:

$$\begin{aligned} \frac{E_{H1}}{J_x} &= m_1 R_3(B) - n_1 R_2(B) \\ \frac{E_{H2}}{J_x} &= n_1 R_1(B) - \ell_1 R_3(B) \\ \frac{E_{H3}}{J_x} &= \ell_1 R_2(B) - m_1 R_1(B) \end{aligned} \qquad (12)$$

The component measured in the y direction is

$$E_{Hy} = \ell_2 E_{H1} + m_2 E_{H2} + n_2 E_{H3} \qquad (13)$$

Substitute the expressions 12 into equation 13 and recall that the

transformation matrix is unitary. Finally one gets

$$\frac{E_{Hy}}{J_x} = -\ell_3 R_1(B) - m_3 R_2(B) - n_3 R_3(B) \qquad (14)$$

With the assumption that equation 8 holds,

$$R_1(B) = R_{1.1}B_1 + R_{1.2}B_2 + R_{1.3}B_3$$

$$R_2(B) = R_{2.1}B_1 + R_{2.2}B_2 + R_{2.3}B_3$$

$$R_3(B) = R_{3.1}B_1 + R_{3.2}B_2 + R_{3.3}B_3$$

But B is directed along the z axis. Therefore

$$B_1 = \ell_3 B_z \quad B_2 = m_3 B_z \quad B_3 = n_3 B_z$$

Thus

$$\frac{E_{Hy}}{J_x B_z} = -\ell_3(R_{1.1}\ell_3 + R_{1.2}m_3 + R_{1.3}n_3) - m_3(R_{2.1}\ell_3 + R_{2.2}m_3 + R_{2.3}n_3)$$
$$-n_3(R_{3.1}\ell_3 + R_{3.2}m_3 + R_{3.3}n_3)$$

or grouping terms in a different way:

$$R_{z.z} = -\frac{E_{Hy}}{J_x B_z} = (\ell_3)^2 R_{1.1} + (m_3)^2 R_{2.2} + (n_3)^2 R_{3.3} + \ell_3 m_3(R_{1.2} + R_{2.1})$$
$$+ m_3 n_3 (R_{2.2} + R_{3.2}) + n_3 \ell_3 (R_{3.1} + R_{1.3}) \qquad (15)$$

This equation relates the Hall coefficient measured as described in section 2.11 and calculated from equation 11 to the galvanomagnetic coefficients. If six independent orientations can be found and $R_{z.z}$

measured for all six orientations, the six independent quantities $R_{k.m}$ can be determined.

2.22 Galvanomagnetic tensors for the point group D_{6h}

Pure titanium has a hexagonal close-packed structure in the temperature range investigated. Its Laue point-group symmetry which determines the number of independent components of the galvanomagnetic tensors is D_{6h} or (6/m) (2/m) (2/m). The principal crystallographic axes are: Ox_1 and Ox_2 parallel to two perpendicular twofold axes; Ox_3 is parallel to the sixfold axis.

As seen in the previous paragragraph, the Hall field E_H can be written as:

$$E_{Hi} = \epsilon_{ijk} J_j R_k(B)$$

with $R_k(B) = R_{k.m} B_m + R_{k.mno} B_m B_n B_o + \ldots$. For the point group of interest the number of components of these two tensors is sufficiently small so that we can write the expressions explicitly. Although it does not come in here, we shall first mention the resistivity tensor $\rho_{ij}(0)$. It has two independent components: $\rho_{11} = \rho_{22} = \rho_\perp$ and $\rho_{33} = \rho_\parallel$. All non diagonal elements are zero.

The tensor $R_{k.m}$ is also diagonal and has two independent components:

$$R_{1.1} = R_{2.2} = -R_\perp \quad \text{and} \quad R_{3.3} = R_\parallel$$

The subscripts $\parallel$ and $\perp$ mean that the magnetic induction B is parallel or perpendicular to the sixfold axis x_3. The tensor $R_{k.mno}$ is more

complicated but the subscripts relative to the magnetic field can be transposed:

$$R_{k.mno} = R_{k.nom} = R_{k.omn} = R_{k.nmo} = R_{k.mon} = R_{k.onm}$$

The components can thus be arranged in a table of three rows (k = 1,2,3) and ten columns, each column corresponding to a different arrangement of the three indices mno.

mno	111	112	122	222	113	123	223	133	233	333
k = 1	$R_{1.111}$	0	$\frac{1}{3}R_{1.111}$	0	0	0	0	$R_{1.133}$	0	0
k = 2	0	$\frac{1}{3}R_{1.111}$	0	$R_{1.111}$	0	0	0	0	$R_{1.133}$	0
k = 3	0	0	0	0	$R_{3.113}$	0	$R_{3.113}$	0	0	$R_{3.333}$

There are four independent components for which we shall use the simplified notation: $R_{1.111} = R_1$, $R_{1.133} = R_2$, $R_{3.113} = R_3$, $R_{3.333} = R_4$. The three components of the Hall vector are then:

$$\begin{aligned} R_1(B) &= -R_\perp B_1 + R_1(B_1^3 + B_1B_2^2) + 3R_2B_1B_3^2 \\ R_2(B) &= -R_\perp B_2 + R_1(B_2^3 + B_2B_1^2) + 3R_2B_2B_3^2 \qquad (16) \\ R_3(B) &= -R_\parallel B_3 + R_4B_3^3 + 3R_3(B_1^2B_3 + B_2^2B_3) \end{aligned}$$

Plug these expressions into equation 14 using also the values of B_1, B_2 and B_3 in terms of B_z.

$$R_H = \frac{E_{Hy}}{J_x B_z} = R_\perp (\ell_3^2 + m_3^2) + R_\parallel n_3^2 - \left[R_1(\ell_3^2 + m_3^2)^2 + 3(R_2 + R_3)(\ell_3^2 + m_3^2)n_3^2 + R_4 n_3^4\right] B_3^2 \qquad (17)$$

All six galvanomagnetic coefficients can be obtained by measuring the Hall coefficient in the usual manner for six different, independent orientations.

A more general form of equation 16 could have been obtained by choosing B in an arbitrary position in the yz plane. B_1, B_2 and B_3 would have been expressed in terms of B_z and B_y instead of just B_z. The expression of R_H would have been more complicated. Furthermore the presence of a component of the magnetic field in the plane of the sample gives rise to the so called "planar Hall effect" which produces an electric field which adds to the proper Hall field.

In order to define the Hall coefficient R_H only the component E_{Hy} has to be considered. However, in anisotropic media the Hall field is not directed in the y direction. It has other components which can be written out in terms of the galvanomagnetic coefficients as well. From equations 12 we can obtain the other two components in the xyz system

$$\frac{E_{Hx}}{J_x} = \ell_1(m_1R_3-n_1R_2) + m_1(n_1R_1-\ell_1R_3) + n_1(\ell_1R_2-m_1R_1) = 0$$

$$\frac{E_{Hz}}{J_x} = \ell_3(m_1R_3-n_1R_2) + m_3(n_1R_1-\ell_1R_3) + n_3(\ell_1R_2-m_1R_1)$$

Using equation 16, E_{Hz} can be written in terms of $R_{\parallel}$ $R_{\perp}$ R_1 R_2 R_3 and R_4 in a straightforward fashion. This component in the z direction is due to the planar Hall effect just mentioned. This effect produces a component in the y direction (which would thus lead to an erroneous Hall coefficient) only if the magnetic induction has a component in the plane of the specimen.

A similar development could have been carried out on the other part of the electric field, namely, $E_{Pi} = \rho_{ij}(B)\, J_j$. Expressions for the magnetoresistance involving $\rho_{ij}\,(0)$ and $\rho_{ij,mn}$ would have been obtained.

2.23 The Voigt-Thomson formula

In the case of titanium the earlier investigations have shown that the Hall effect is strictly proportional to the magnetic field. It is therefore adequately described with only the first order galvanomagnetic coefficients. Equation 8 can be used, or equation 3, which is equivalent. Combining this equation with the results of the previous section, we shall develop a very simple formula for the Hall coefficient. Following Okada's analysis we write the Hall field

$$E_{H1} = -J_2 R_{\parallel} B_3 + J_3 R_{\perp} B_2$$

$$E_{H2} = -J_3 R_{\perp} B_1 + J_1 R_{\parallel} B_3$$

$$E_{H3} = -J_1 R_{\perp} B_2 + J_2 R_{\perp} B_1$$

By carrying out the same steps that lead to equation 15 or applying this equation directly, we obtain

$$R_H = \frac{E_{Hy}}{J_x B_z} = (\ell_3^2 + m_3^2)\, R_{\perp} + n_3^2 R_{\parallel} \qquad (18)$$

This follows also from equation 17 where one sets $R_1 = R_2 = R_3 = R_4 = 0$. In Kohler's treatment, the Hall field is written

$$E_{Hi} = R_{ik\ell}\; J_k B_\ell$$

For the point group D_{6h} the tensor $R_{ik\ell}$ has only six non zero components

of which only two are independent.

$$R_{123} = -R_{213} = -R_{\parallel} = R_{3.3}$$

$$R_{132} = R_{321} = -R_{231} = -R_{312} = -R_{1.1} = -R_{2.2} = R_{\perp}$$

The components of the Hall field are then:

$$E_{H1} = R_{123}J_2B_3 + R_{132}J_3B_2$$

$$E_{H2} = R_{231}J_3B_1 + R_{213}J_1B_3$$

$$E_{H3} = R_{312}J_1B_2 + R_{321}J_2B_1$$

By replacing the R_{ijk} in terms of $R_{\parallel}$ and $R_{\perp}$ we obtain exactly the same expressions for E_{Hi} as above. Experimentally one measures E_{Hy} with $J_y = J_z = 0$ and $B_x = B_y = 0$. Then

$$E_{Hx} = 0$$

$$E_{Hy} = R_{yxz}J_xB_z$$

$$E_{Hz} = 0$$

The Hall coefficient determined experimentally is therefore R_{yxz}. It is related to $R_{\parallel}$ and $R_{\perp}$ by the transformation law of the third rank tensors:

$$R_{yxz} = n_3(m_1\ell_2 - \ell_1m_2)R_{\parallel} + m_3(\ell_1n_2 - \ell_2n_1)R_{\perp} + {}_3(n_1m_2 - n_2m_1)R_{\perp}$$

or

$$R_{yxz} = R_H = n_3^2R_{\parallel} + (m_3^2 + \ell_3^2)R_{\perp} \qquad (19)$$

which is of course identical with equation 18.

Describe the relationship between the xyz and $x_1\ x_2\ x_3$ systems by means of the Euler angles $\phi\ \omega\ \psi$ (Fig. 4). ϕ is the rotation of $x_1\ x_2\ x_3$ about Ox_3 bringing Ox_2 into Oy'. ω is the rotation of the new system about Oy' which brings Ox_3 into Oz. ψ is a rotation about Oz bringing Oy' in coincidence with Oy. Under these circumstances, the direction cosines of Oz with respect to the $x_1\ x_2\ x_3$ system are:

$$\ell_3 = \sin\omega\cos\phi;\ m_3 = \sin\omega\ \sin\phi;\ n_3 = \cos\omega$$

Substituting these values into equation 18 we obtain the well-known Voigt-Thomas formula

$$R_H = R_{\parallel}\ \cos^2\omega + R_{\perp}\ \sin^2\omega \qquad (20)$$

where ω is the angle between the magnetic field (Oz) and the principal axis of the crystal (Ox_3). This is the formula that we will use later to determine $R_{\parallel}$ and $R_{\perp}$ from measured R_H.

Consider now the planar Hall effect. In the Okada formulation

$$E_{Hz} = R_{y.z}J_xB_z = (\ell_2\ \ell_3 + m_2m_3)R_{\perp} + n_2n_3R_{\parallel}$$

If the medium were isotropic $E_{Hz} = (\ell_2\ \ell_3 + m_2m_3 + n_2n_3)\ R = 0$. In the Kohler formulation, however, we have just seen that $E_{Hz} = 0$ even for non isotropic media. This method is therefore restricted to the proper Hall effect and has less generality.

2.3 Conventional Method of Measuring the Hall Effect

The Hall effect was first measured using a rectangular sheet sample. The geometrical arrangement of current, magnetic field and potential

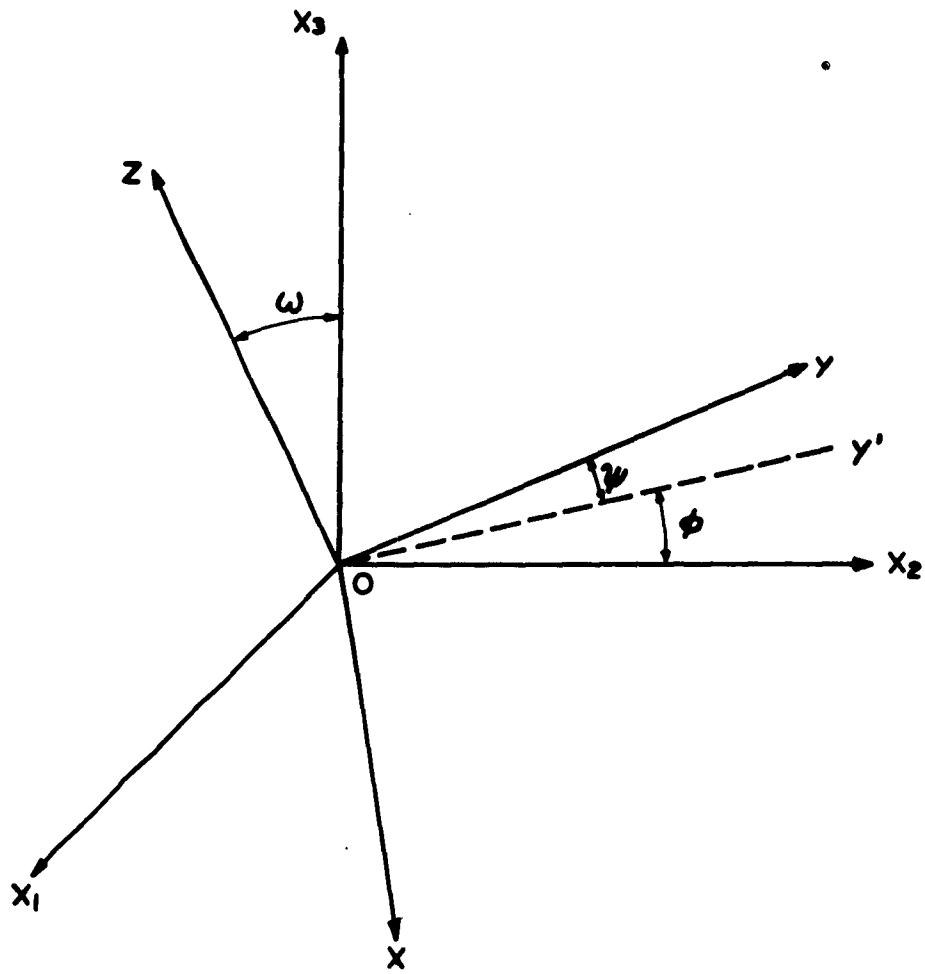

Fig. 4. The two systems of coordinates attached to a single crystal Hall plate. Euler angles

xyz: edges of the plate
$x_1x_2x_3$: crystallographic axes

probes is sketched in Fig. 5. This conventional method using direct current is still much in use and has been chosen in this study. It will therefore be discussed to show its principal features and limitations.

2.31 Experimental conditions

If the voltage measured between A and B is to represent truly the Hall effect, a certain number of experimental requirements have to be satisfied. Different results are obtained depending on whether the measurement is carried out under isothermal or adiabatic conditions. In the absence of special precautions, the voltage between A and B is the combined result of several galvanomagnetic and thermomagnetic effects. Only if the temperature is maintained uniform and constant, the true isothermal Hall effect is measured and the results of section 2.2 are applicable. In practical situations, however, a longitudinal temperature gradient is produced at the current electrodes E and F by the Peltier effect. The electrodes are usually of copper; not the same material as the sample. One end is warmed, the other cooled producing a heat flow along the plate. Arising from this gradient, the Nernst effect produces a transverse emf which is measured together with the Hall voltage. A transverse temperature gradient is also established. It has its origin in the Ettingshausen effect of the electrical current and the Righi-Leduc effect of the longitudinal temperature gradient[8].

If the Hall probes are of a material different from the sample, these temperature gradients produce a thermoelectric potential difference which reverses with current and magnetic field in the same way as the Hall voltage. If one measures a Hall current instead of the voltage,

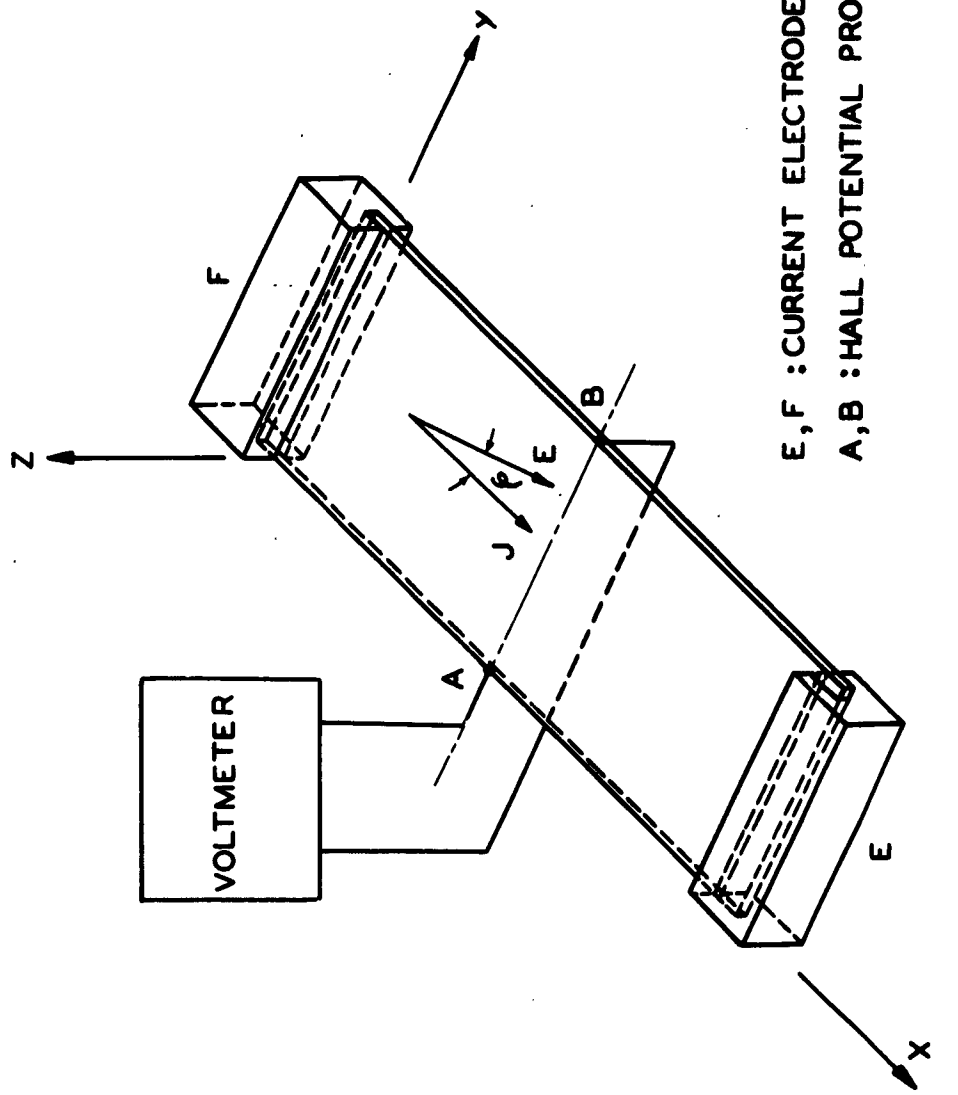

Fig. 5. DC method of Hall effect measurement (schematic).

this current generates a transverse Peltier effect, thus changing the temperature gradient due to the Ettingshausen effect. To eliminate most of these errors or reduce them to an acceptable level, one can choose among the following remedies:

a. eliminate the current contacts by using induced currents,

b. measure the Hall voltage by a null method (compensation method),

c. reverse I and B rapidly: temperature gradients reverse more slowly than the Hall field,

d. thermoelectric voltages do not reverse with the current and are eliminated by reversing the current and averaging,

e. use Hall probes of the same material as the sample: then no thermal emf appears due to the Ettingshausen effect and no Peltier effect due to the Hall current,

f. most of the spurious emfs can be avoided by placing the sample in an isothermal bath. They can also be eliminated by combining reversal of the current and the magnetic field.

In practice a compromise has to be found such that the effects not eliminated are negligible or can be compensated for. The observed voltage is thus very close to the isothermal Hall voltage even though the conditions may not be perfectly isothermal.

If the voltage appearing between A and B when the magnetic field is turned on has to be due only to the Hall effect, in addition to the precautions mentioned above, one has to realize zero potential difference between A and B in zero magnetic field. If this is not the case, the

small voltage existing before the field is turned on will be affected by the magnetic field and a part of the longitudinal effect is incorporated in the Hall measurement. It is therefore recommended to align A and B on the same equipotential before B is applied. Only then $V_y(B)-V_y(0)$ is a good measurement of V_H. The small contribution of the longitudinal magnetoresistance can be eliminated by averaging $V_y(B)$ and $V_y(-B)$ or by using a three probe geometry (see section 3.23 below).

2.32 Corrections due to the size of the specimen

So far the Hall effect has been described for homogeneous samples. Corrections may be necessary when working with an inhomogeneous conductor. In the case of iodide titanium we shall assume that this consideration can be left out, the samples being homogeneous and pure enough. Other requirements for a valid application of the formulas given in section 2.1 are more difficult to satisfy. They concern mostly the dimensions of the sample. The lines of primary current flow must be parallel. This is true only if the plate is infinitely long and of uniform thickness.

Two sources of error are related to the thickness. A nonuniform thickness makes the interpretation of the Hall coefficient measurements very difficult. It is then more satisfactory to measure the Hall angle which is not dependent on the uniformity of the plate surface. For very thin samples there is in addition a size effect due to the scattering at the surface of the specimen. This effect has been observed in several cases but is not well accounted for by theories. We shall discuss it later more specifically.

The measured potential difference between A and B has to be multiplied by a dimensionless factor f(u) in order to obtain the Hall voltage. This is a result of the shorting out effect of the current electrodes: the copper current electrodes along the short sides of the Hall plate act as a short circuit on the Hall probes. The correction factor f(u) is a smooth function of the parameter $u = tr/\rho_o$; ρ_o is the zero field electrical resistivity, t the thickness of the plate and r its resistance between E and F. For a rectangular plate it is the ratio $u = \ell/b$ of length to width.

u	.5	1.0	1.5	2.0	2.5	3.0	4.0	∞
f(u)	.370	.675	.847	.923	.967	.984	.996	1.000

This calculation assumes that the electrical resistance of the current electrodes is much smaller than the resistance of the plate and that the Hall angle is sufficiently small in order that $\tan^2\varphi$ be much less than 1.

Since the Hall probes cannot be soldered right at the edge of the sample, the effective width b of the plate is reduced near the probes. The measured value is larger than the true Hall voltage[11]. The correction depends on the ratio of the length of one junction to the total width of the plate.

Most of these corrections are sufficiently small in the practical arrangement chosen so that they can be neglected.

2.33 Other sources of error

Many other sources of error are introduced either by the method itself or by the conditions of its performance. Surface conductivity,

field homogeneity, surface roughness are such factors. The magnitude of the errors introduced can be estimated from calculations or models presented in the literature. Hereafter we shall neglect them completely.

As an example of the kind of errors neglected, a second order effect of anisotropy in the electrical conductivity is now described. Consider a single crystal in the shape of a rectangular plate with the usual probe geometry. In the absence of the magnetic field, the electric vector $\vec{E}$ is at an angle δ from the current density $\vec{J}$ (Fig. 6). The Hall probes are adjusted so as to be on the same equipotential line, which makes an angle δ with the y direction in which the Hall voltage V_{Hy} should be measured. When the magnetic field is turned on, the angle between E and J becomes $\delta' = \delta + \varphi$, where φ is the Hall angle. What is called the Hall voltage and is described by the formalism developed in paragraph 2.23 is

$$V_H = V_{B_1}(H) - V_{B_1}(0)$$

Neglecting second order effects like magnetoresistance, the electric vector E has the same length whether B is zero or not. Then

$$V_{B_1}(0) = V_B(0) + Ed$$

where d ($d = b \sin\delta$) is the normal distance between the equipotentials of B and B_1. Similarly, $V_{B_1}(H) = V_B(0) + Ed'$ with $d' = b \sin\delta'$. Then

$$V_H = Eb(\sin\delta' - \sin\delta)$$

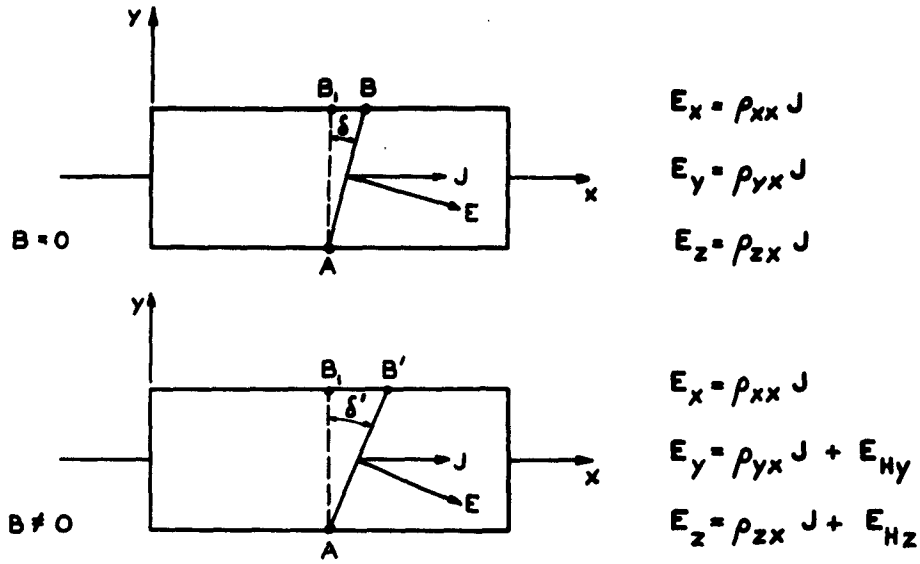

RELATIONSHIP BETWEEN $\vec{E}$ AND $\vec{J}$ IN A SINGLE CRYSTAL HALL PLATE

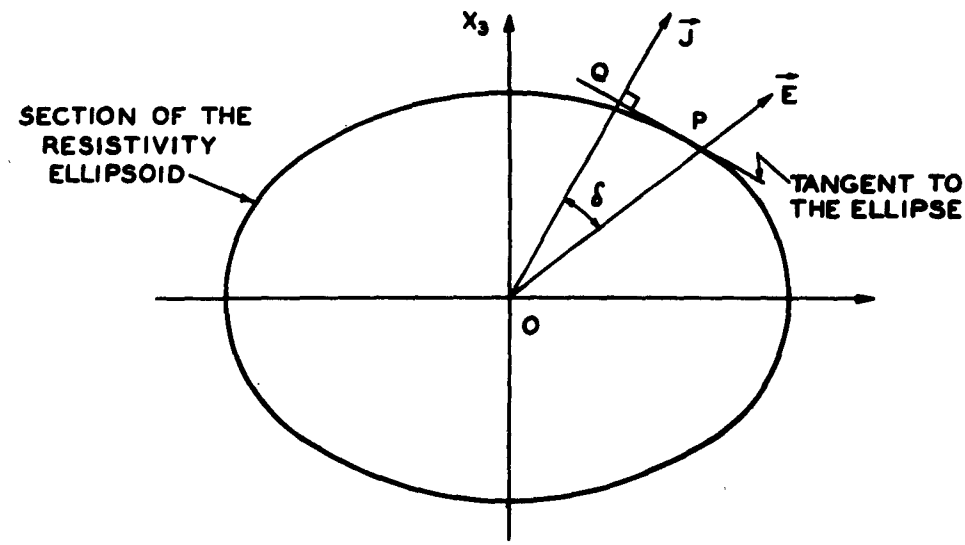

Fig. 6. Relationship between electric field and current density in a single crystal plate magnetic field.

The experiment, however, yields

$$V_H' = V_B(H) - V_B(0) = Eb \frac{\sin\varphi}{\cos\delta}$$

The error $\Delta V_H = Eb \left[\sin(\delta + \varphi) - \frac{\sin\varphi}{\cos\delta} - \sin\delta \right]$ vanishes in the first order. The small magnitude of the error arises from the fact that δ is very small for titanium. This is best seen from the construction in Fig. 6 using the resistivity ellipsoid $(x_1 / \rho_\perp)^2 + (x_2 / \rho_\perp)^2 + (x_3 / \rho_\parallel)^2 = 1$. It can also be obtained from $\tan\delta = E_y/E_x = \rho_{yx}/\rho_{xx}$, ρ_{yx} a nondiagonal term in the conductivity tensor is small. Since $\rho_\parallel$ and $\rho_\perp$ are nearly equal for titanium, the ellipsoid of resistivities is almost a sphere[12] and its tangent in P is almost normal to OP. Thus P and Q are very close. The use of V'_H instead of V_H to calculate the Hall field E_{Hy} does not introduce a noticeable error and the values obtained in this manner for $R_\parallel$ and $R_\perp$ will be satisfactory.

2.4 Other Methods

In order to avoid the sources of error which accompany the DC method, other geometries and other techniques have been used to measure the Hall effect.

2.41 Alternating current methods

An AC Hall voltage can be obtained by using AC current and DC magnetic field, DC current and AC magnetic field or AC current and AC magnetic field of different frequencies[13]. This voltage can be directly amplified and recorded after calibration of the apparatus by a

known test signal. Saturation of the amplifier by the misalignment voltage must be avoided: there should be zero voltage between A and B in the absence of magnetic field. The use of an AC compensation method gives both amplitude and phase of the Hall voltage and thus the sign of the Hall coefficient can be found by comparing this phase with that of the primary current. The main advantage of the method is to yield directly the isothermal Hall coefficient, the thermal emfs being eliminated. Difficulties arise, however, from noise and stray voltages. Shielding and grounding must be used and vibrations induced by the magnetic field in the leads must be prevented. In practice it is therefore hard to separate extraneous voltages from the quantity of interest.

2.42 Methods using systems with cylindrical symmetry

a. The sample is a flat disc perpendicular to a uniform magnetic field. The primary current is radial. The Hall effect produces a circular current. This is called the Corbino effect and it yields a value for the Hall angle.

b. A uniform magnetic field which varies with time induces circular currents in a flat disc. A radial Hall field appears. This method can take advantage of very high pulsed magnetic fields. The Hall voltage pulse between the center and the circumference is

$$\int_0^\infty V_H dt = \frac{-M_0^2}{8} R_H \varphi r^2 B^2$$

when B is varied rapidly from 0 to a maximum value of B.

c. Radial magnetic fields can be used in conjunction with hollow cylindrical specimens. An induced circular current creates an axial

Hall field or, in another version, an axial current causes a circular Hall current.

Many other ingenious arrangements or variations on the described ones can be imagined and may present advantages over the conventional method in the particular case considered.

3. EXPERIMENTAL APPARATUS AND METHODS

In this investigation a DC method is used to measure the Hall effect. Only this method has a sensitivity of the order of 5×10^{-9} volts which is required to obtain the Hall voltage with reasonable accuracy. Furthermore this method has been shown to be successful in similar investigations and has the additional advantage of being very simple in principle.

The governing factor in the design of the measuring circuit is the magnitude of the voltage to be detected. If a specimen of $2 \times 4 \times .005$ inches is used, when traversed by a current of one ampere in the presence of a magnetic field near ten kilogauss, it exhibits at room temperature a Hall voltage of only 2.5×10^{-7} volts. The measurement of such small voltages calls for special care in the design of the apparatus.

3.1 Experimental Arrangement

The photograph on the following page (Fig. 7) shows the experimental arrangement used for the measurement of resistivity and Hall coefficient of a titanium sample, from liquid helium temperature to room temperature. The specimen is located in the gap of an electromagnet, inside a double metallic Dewar vessel. Electrical leads carrying the current or belonging to various circuits connect the specimen to power supply and measuring instruments,

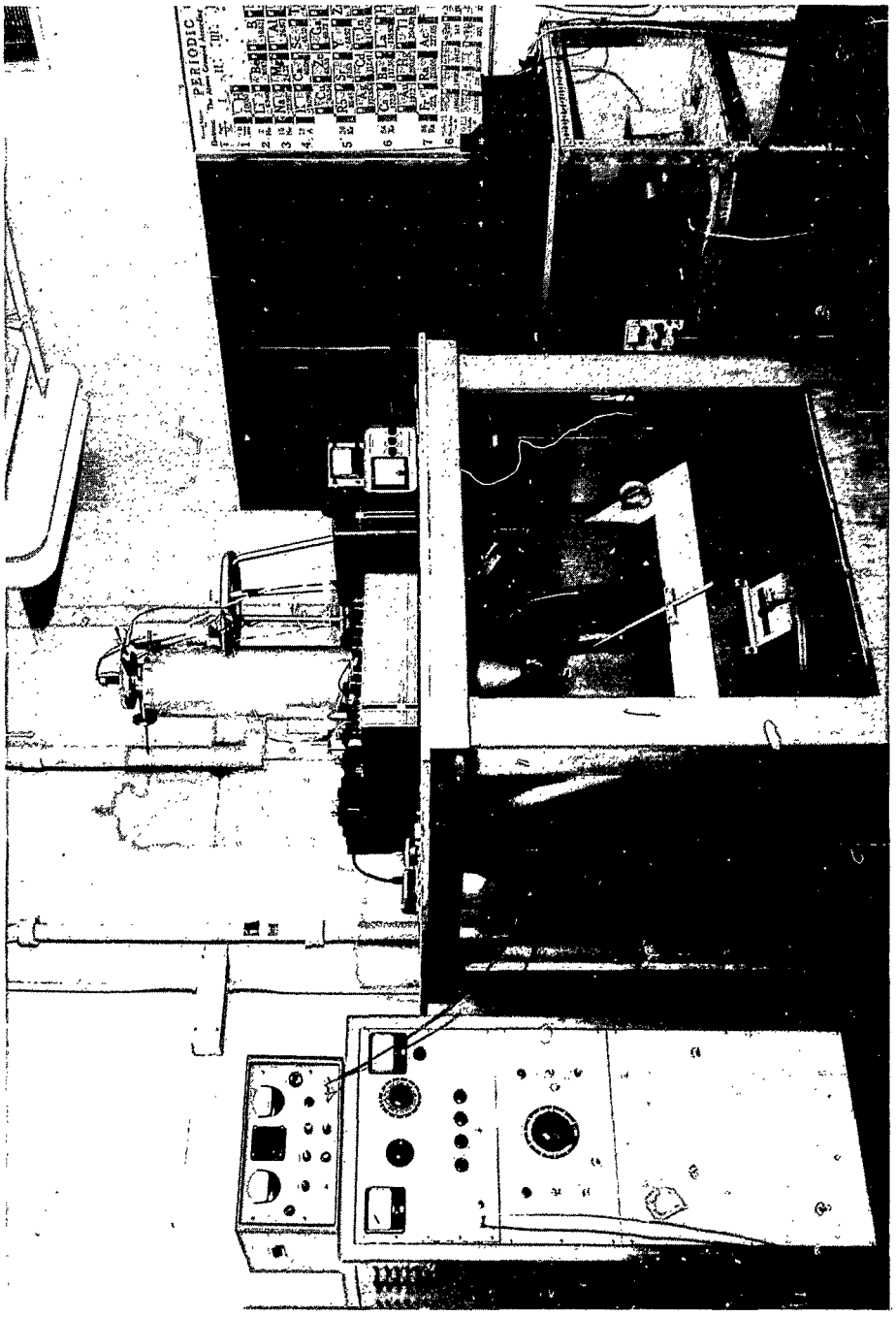

Fig. 7. General view of the experimental assembly.

mostly potentiometers. These circuits allow the measurement of the Hall voltage after partial amplification and of the other quantities of interest: current, temperature, resistivity. In the photograph one can also see the magnet power supply and the nuclear fluxmeter used to measure the strength of the magnetic field.

3.2 The Electrical Circuit

The electrical circuit used to determine Hall coefficient and resistivity is depicted schematically on the diagram of Fig. 8.

3.21 Specimen and specimen holder

The specimen is a thin rectangular sheet of titanium of about 12 cm long, 4 cm wide and .01 cm thick. The current electrodes E and F are along the short sides of the plate. The correction for finite length is small in this case: $u = \ell/b$ is near 3 and the corresponding correction factor f(u) is 0.98. This factor has been calculated by assuming the electrical resistance of the current electrodes, two copper strips, much smaller than the resistance of the sample and the Hall angle such that $\tan^2\varphi$ is much less than one (in titanium $\tan\varphi \simeq 4 \times 10^{-4}$). These conditions are satisfied. Furthermore for the thickness chosen, no appreciable size effect is expected, if titanium behaves in a manner very similar to other metals.

The specimen is attached to a bakelite holder which serves as a support for the sample itself as well as for the electrical connections and leads. It is shown in Fig. 9. One end of the sample is clamped against the holder by means of the current electrode, the other end is free. The long sides of the specimen are maintained against the bakelite

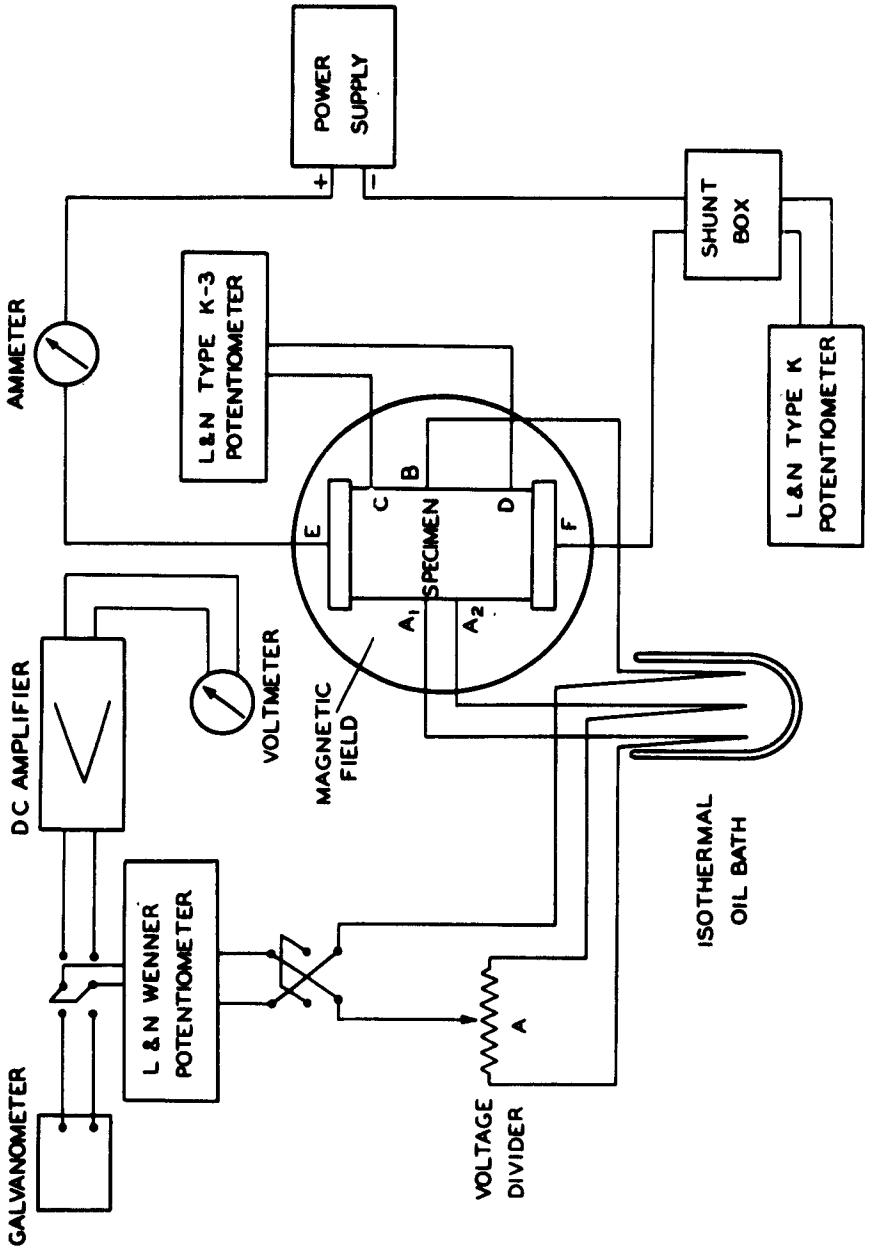

Fig. 8. Schematic diagram of the circuit for the measurement of Hall effect and resistivity.

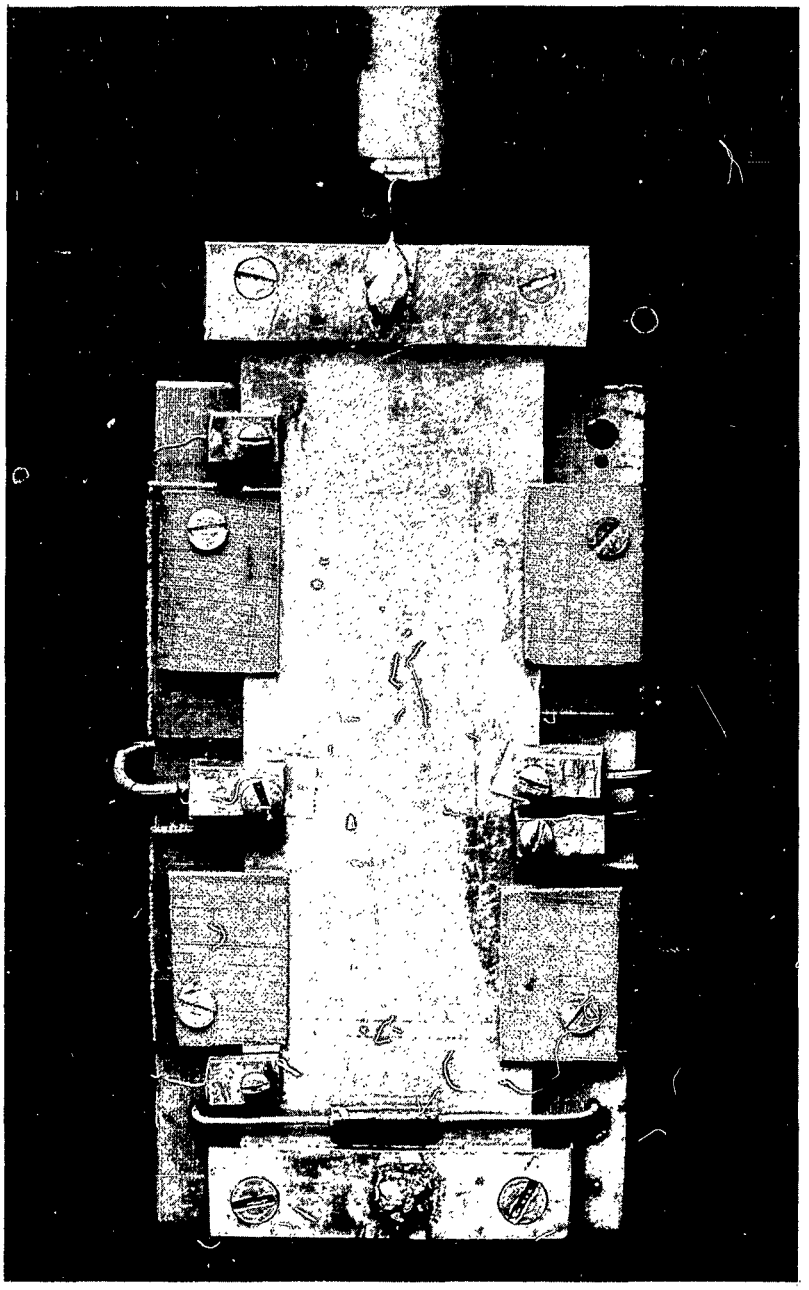

Fig. 9. Specimen of titanium mounted on its holder for Hall coefficient and resistivity measurements.

holder by small pieces of bakelite tightened by brass screws. However the specimen can contract or expand without being restrained by the holder. No stresses are thus introduced when it is cooled down. The specimen and its holder are wrapped in a thin sheet of insulating material (mylar), to prevent any metallic part from coming into contact with the cryostat and to avoid a leakage or a short circuit.

3.22 Circuit for the measurement of resistivity

This circuit provides the current I through the specimen and allows measuring it. The addition of two potential probes C and D provides a four-lead potential-terminal resistance circuit. The DC current is obtained by connecting the electrodes E and F in series with a portable transistorized power supply (Universal Electronics Company, model L 3501). This power supply can be utilized as a source of constant current. The output voltage is regulated and changes by only 5 mV per 10% line change. The ripple has an rms of less than 500 microvolts. There is a slow drift, of the order of 20mV, over a period of eight hours. The warm up takes twenty minutes. A switch is provided to open the circuit and to reverse the direction of the current. The current can be varied from 0 to 1 ampere. An ammeter in series in the circuit gives a coarse reading of its value. A more accurate measurement is achieved by placing the Leeds and Northrup shunt box (Catalog No. 4385) in series in the circuit and measuring the voltage drop in the shunt with a Leeds and Northrup potentiometer of type K (Catalog No. 7552). The current is then obtained by multiplying the reading of the potentiometer by the factor appearing on the range dial of the shunt box. The Leeds and Northrup type K potentiometer allows to measure voltages from 0 to 1.6 volts with four

significant figures. The current leads are of copper and their diameter is chosen such as to minimize the total amount of heat that they introduce into the Dewar through Joule effect and heat conduction. The use of electrodes covering the whole width of the specimen favors a uniform current density within the sample. J has therefore a constant value and is directed along the x axis, especially near the center of the specimen, where the Hall probes are located.

The resistivity of the specimen is obtained indirectly by measuring the voltage drop between the points C and D located on the longer side of the plate, a distance ℓ apart. The resistivity potential probes consist of two small copper clamps, making almost a point contact with the specimen through a small brass screw. A thin sheet of mylar isolates the titanium sheet from the copper clamp itself. C and D are located a certain distance away from the ends of the plate, where end effects are no longer felt and J has reached a uniform distribution. The voltage drop V_{CD} between C and D is measured by a compensation method using a Leeds and Northrop type K-3 potentiometer (Catalog No. 7553). The null detector is a galvanometer (L&N No. 2430). The voltage to be balanced with the potentiometer is in the millivolt region. It is most accurately measured when the highest sensitvity range is used (0 to .016110 volts). Then the precision of the reading is $\pm$ (.015% + .5μV), including uncertainties in measuring and standardizing. The potentiometer has a "reverse emf" position, making possible the measurement of voltages of both signs without changing the lead connections.

3.23 Circuit for the measurement of the Hall voltage

The DC voltage, developed by the shift in the equipotential lines and due to the magnetic field, can in principle be measured by just adding two potential probes across the specimen in the y direction. Owing to the small magnitude of the effect, the presence of parasitic voltages and their dependence on all experimental variables (current, magnetic field, temperature, contact potentials), special care must be taken in mounting the probes. Following the conclusions arrived at in section 2.3, titanium wires are taken as potential leads in order to eliminate thermal emfs due to several transverse effects, when the specimen is not placed in an isothermal bath. In order to be able to align the two probes A and B on the same equipotential line in the absence of the magnetic field, the following probe geometry is used. One one side of the specimen, probe A is replaced by two probes A_1 and A_2, about 5 mm apart and located on opposite sides of the equipotential of B. A_1 and A_2 are connected to a 10 ohm voltage divider with a fine adjustment (a 10 ohm Beckman Helipot). A is then the point on the slider of the Helipot. The voltage V_{AB} can thus be varied continuously between V_{A_1B} and V_{A_2B} and brought down as close to zero as the fineness of the divider can permit. This adjustment is most sensitive if the separation between A_1 and A_2 is small: a distance of 5 mm is sufficient, because it allows room for the probes and makes it relatively easy to locate A_1 and A_2 on opposite sides of the equipotential of B. This method has two perturbing effects on the measurement. First, it causes a modification of the current distribution in the sample near the Hall probes: a small current circulates through the

Helipot, in parallel with the sample between A_1 and A_2. This current, however, is very small in comparison to the current through the specimen, the ratio of the resistances of the two branches being about 10^4. For practical purposes the current lines in the titanium plate can be considered as unaffected. The second effect of the three probe geometry is a change in the sensitivity of the Hall measurement itself.

Fig. 10 represents an "equivalent" or reduced diagram of the Hall voltage measuring circuit. The alignment of the probes is realized when

$$\frac{r}{r'} = \frac{R}{R'}$$

Call E_P the voltage at the terminals of the potentiometer, V_H the Hall voltage. If perfect balance is realized, $E_P = V_H$ and there is no error. If there is a slight difference between E_P and V_H, corresponding to one division of the finest decade of the potentiometer, a current i will circulate in the whole circuit: $V_H - E_P = (P + r'' + R_e)\, i = V$. R_e is the resistance equivalent to the net R, R', r, r'. It is given by:

$$R_e = \frac{(R + r)(R' + r')}{R + R' + r + r'}$$

The actual values of the various resistances involved in these formulas make it possible to simplify the equations by neglecting smaller terms. Resistances in the sample itself, r, r', r", are fractions of a milliohm. Resistances in the Helipot, R and R', are much larger (R + R' = 10 ohms). The value of P, the resistance of the leads and the internal resistances of the potentiometer and the galvanometer, is about 30 ohms. If A_1 and A_2 are symmetrically located with respect to B, R and R' equal 5 and R_e equals 2.5 .

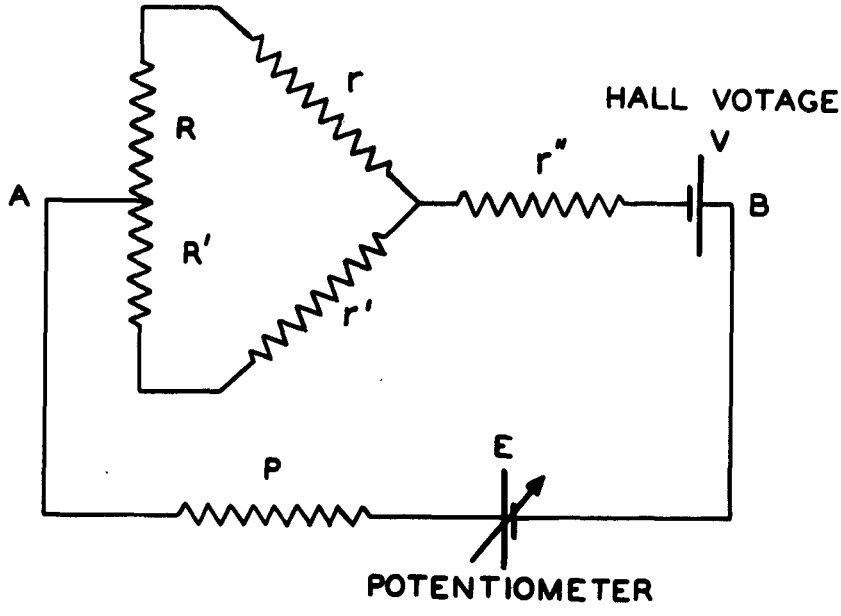

Fig. 10. The three probe geometry. Equivalent diagram.

The current i produces a deflection of the galvanometer corresponding to a voltage $\Delta E_P = Pi = \frac{P}{P + R_e} \Delta V$

The value read with the potentiometer and the galvanometer for the Hall voltage is then $V'_H = E_P + \Delta E_P$ instead of the actual value of $V_H = E_P + \Delta V$. The error is minimum if $\frac{\Delta E_P}{\Delta V} = \frac{1}{1 + R_e/P}$ is as close to 1 as possible.

Since P is given, this condition requires R_e to be small. For the Helipot used,

$$R_e = 2.5\Omega \text{ and } \frac{\Delta E_P}{\Delta V} \simeq .90$$

It is much easier to make this correction, than to evaluate the perturbation introduced by a non uniform current, which would exist if the Helipot had a much smaller resistance.

The error on the Hall voltage itself is $\frac{V_H - V'_H}{V_H} = \frac{0.10\,\Delta V}{E_P + \Delta V}$

In the actual case $\Delta V = .05\mu V$ and $E_P \simeq .25\ \mu V$. The error is then about 2% and the observed value is less than the actual voltage. This factor compensates almost exactly for the effect of the finite length of the plate.

An additional advantage of the three probe geometry is that it eliminates the effect of fluctuations of the primary current on the Hall measurement. If the probes are not aligned, there is a bias voltage superimposed on the Hall voltage, which is proportional to J and fluctuates with it. Averaging V_{AB} (B) and V_{AB} (-B) does not get rid of the

fluctuating part of this voltage. When the probes are aligned, this bias voltage stays zero whatever J does. The practical realization of this circuit is now presented.

At points A_1 A_2 and B titanium wires are clamped onto the specimen by means of brass screws. Electrical contact with the specimen is established by spot welding or just pressing the leads against the specimen. Special care is taken to prevent any contact of the clamp or the tightening screw with the titanium lead and the sample. Outside the Dewar, the titanium leads are changed to copper in an isothermal oil bath. Two copper leads connect then the slider of the Helipot and the lead coming from B to the emf terminals of a Leeds and Northrup Wenner potentiometer (catalog No. 7559). This instrument measures low DC voltages with high accuracy and reliability. The design largely overcomes inevitable parasitic emfs and resistance variations at the adjustable contacts. The null detector is a Leeds and Northrup 2284-c reflecting galvanometer with a sensitivity of 0.1μV/mm on the scale. In the low range, voltages from 0 to .011111 volt can be measured to the nearest 0.1 μV. Interpolation on the scale permits readings to be made within 0.01 μV. The systematic errors due to constuction, calibration and standardization are ± .01%. To improve the accuracy of the measurement, the Hall voltage is first balanced to the nearest 10^{-7} volt with the Wenner potentiometer. The remaining voltage, less than 10^{-7} volt, is amplified by a Beckman Model 14 DC breaker amplifier and read on a Du Mont vacuum tube voltmeter (type 405). The method is no longer a perfect null measurement, but the errors introduced are negligible. A two position switch allows to direct the

output of the Wenner potentiometer either toward the galvanometer or the amplifier. A similar switch is provided on the input connections to the potentiometer, to enable the measurement of voltages of both signs.

The amplifier is designed for the measurement of voltages in the microvolt and fractional microvolt region. It has a noise level within a factor of 2 of the theoretical Johnson noise (maximum noise 3×10^{-9}, rms 1×10^{-9} volt). Input signals up to 300μV may be applied without overloading. The whole Hall signal could therefore be amplified. However the sensitivity would be much smaller and the output voltage would no longer be proportional to the input, as can be seen from the output characteristics (Fig. 11). The system can be calibrated by means of a test signal control on the amplifier, or by making 10^{-7} volt changes by rotating step by step the last decade dial of the Wenner potentiometer. A zero positioning control is provided for bucking out residuals in the input circuit. The instrument has a warm-up period of one hour and a drift of less than .005μV per day. It has good signal to noise ratio, provided the input circuit has an impedance between 7 and 60 ohms (nominal impedance: 20Ω, impedance of the actual circuit 25Ω).

In order to take advantage of the full sensitivity and accuracy of the amplifier, an all copper circuit is used and special solder is employed to avoid thermal emfs as much as possible. To prevent unwanted electromagnetic signals from being picked up, the two input leads are kept close together and unnecessary loops are avoided. The pick up is further reduced by shielding the whole circuit, the metallic Dewar being

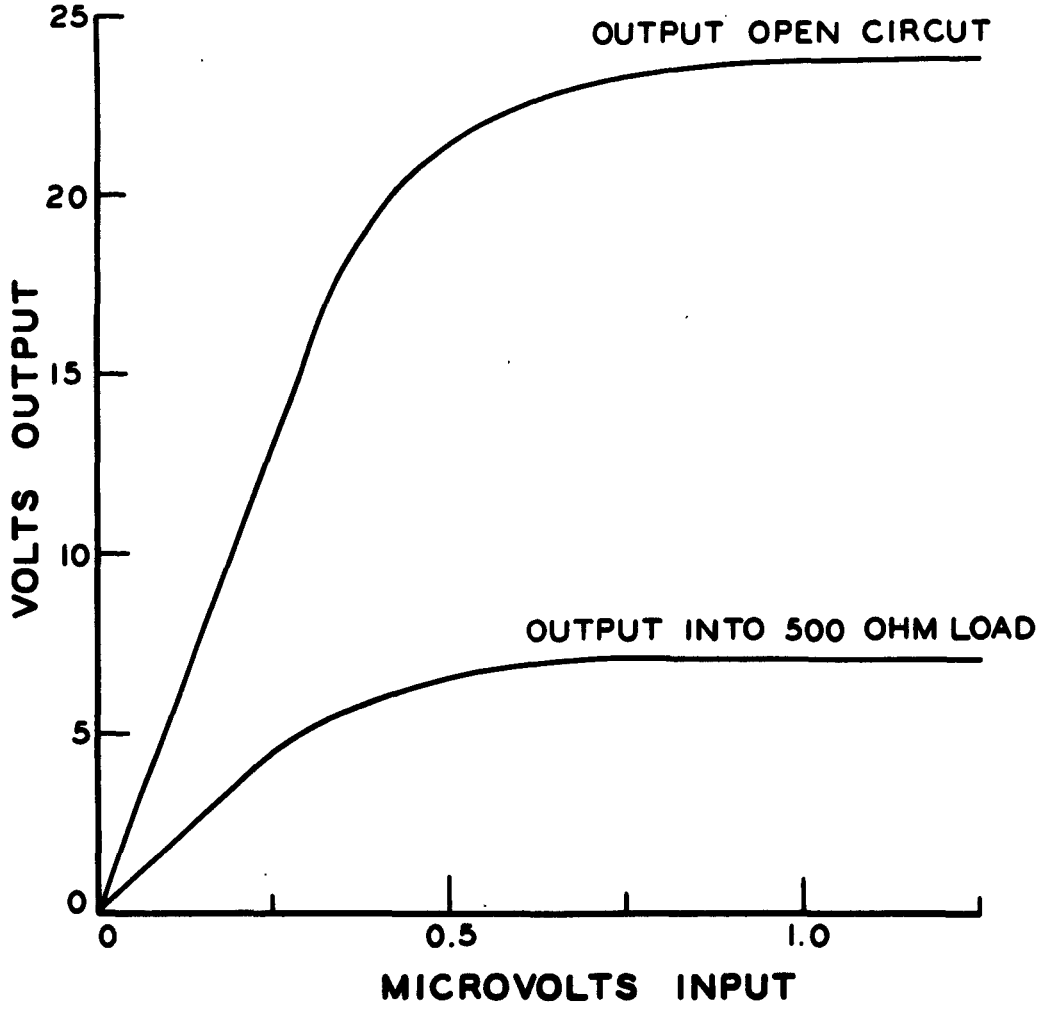

Fig. 11. Output characteristics of the Beckman Model 14 DC Breaker amplifier.

part of the shielding. Nevertheless, a noise level as high as .005μV was left and had its origin mostly in the potentiometer and the Helipot. The latter, not being of copper, also introduced thermal drifts. Additional precautions consisted in avoiding electrical leakage between various elements, including the ground, and mounting the lead wires fairly rigidly inside the bakelite tube and on the specimen holder, thus reducing induced voltages in the measuring circuit caused by vibrations or small magnetic field variations. The output at maximum gain of the amplifier could be conveniently measured on the 10 volt scale of the voltmeter and the vibrations of the needle about its mean position gave an indication of the noise and pickup in the circuit.

3.3 The Magnet System

The magnetic field used in this study was obtained from a Varian twelve inch electromagnet. The complete magnet system is now described.

3.31 The magnet and its power supply

The twelve inch electromagnet system provides an exceptionally stable magnetic field. The model V 4012-3 B electromagnet is capable of supplying large volumes and magnitudes of uniform magnetic field as required in this study. The magnet is equipped with cylindrical, ring-shimmed pole pieces, which give maximum uniformity of the field. In the central section of the gap, the field is uniform within 1 part in 30,000 over an area of 4 1/2 inches in vertical and 4 inches in horizontal extend. The specimen is entirely located in this region. The air gap between the pole pieces is 2.75 inches and the maximum field of 10.2 kilogauss can be reached for a magnet current of 2.0 amperes per

winding section.

The model V 2100 B regulated magnet power supply generates highly regulated direct current. It is possible to stabilize the current even further using the feedback of a signal derived from a NMR signal. The output can be varied from 0.02 to 2.0 amperes. The regulation of the output current against input line voltage changes or magnet load resistance changes of 10% is as good as one part in 100,000. The direction of the magnetic field can be automatically reversed from the operating panel of the power supply thanks to a field reversing mechanism installed in the power supply.

3.32 Measurement and control of the magnetic field

The magnetic field in the central section of the gap, where the specimen is located, is determined by means of the Varian F8 nuclear fluxmeter. This instrument is designed for accurate measurement and control of magnetic fields from 1 to 52 kilogauss. It operates on the principle of nuclear magnetic resonance. A sample of protons or deuterons, the nuclear resonance characteristics of which are accurately known, is brought to magnetic resonance by the simultaneous application of a known, variable frequency, rf field and the magnetic field to be measured. The frequency of the rf field is varied until a nuclear resonance signal is induced, or alternately, the magnet current is increased until resonance occurs for a preselected frequency. The rf tuning dial provides the operator with a direct read out of the magnetic field in gauss. A discriminator circuit in the fluxmeter functions to keep the magnetic field constant by automatically adjusting the power input to the magnet coils,

in the event of line voltage fluctuations or thermal variations.

There are more accurate ways to interpret the resonance signal than just reading the tuning dial (± 5% uncertainty). An additional scale, a logging scale, is provided on the tuning dial. Careful reading of this scale in conjunction with the calibration curves furnished with the fluxmeter permits measurements accurate within ± 0.2%. It is possible to achieve even more accurate measurements by monitoring the transmitter frequency with an external frequency measuring device. By this method, field intensity in gauss may be measured within ± 0.05 gauss. The proton sample has a resonance frequency of 4.2577 megacycles per kilogauss and is useful for fields between 1 and 8 kilogauss. The deuteron sample has a NMR frequency of 0.6536 megacycles per kilogauss and covers the range from 6.8 to 52 kilogauss.

Accurate determination of the magnetic field is only meaningful if the field is uniform and has the same value at the point where it is measured and in the specimen. In order not to perturb the field homogeneity attained by the equipment just described, no ferromagnetic nor strongly para- or diamagnetic materials are used in the construction of those parts of the apparatus that are located in the gap of the magnet. Only brass, copper and bakelite are used. Titanium itself has a susceptibility of 1.5×10^{-6} C.G.S. and there is no detectable discrepancy between the magnetic induction in the sample and at the location of the NMR probe.

3.4 The Cryostat

In order to make possible measurements of the Hall coefficient and

conductivity over a wide range of temperatures, a liquid helium cryostat has been designed and constructed. It is diagrammed in Fig. 12.

3.41 Description and operation

The cryostat consists of two metallic, coaxial Dewars. Each Dewar is made of a stainless steel cylinder, terminated by a copper part with rectangular cross section, to fit into the air gap of the electromagnet. Each vessel has a double wall, the shell or jacket left in between being evacuated under normal operating conditions. High vacuum valves are provided to allow reevacuation before every low temperature test or as often as necessary. A metallic cryostat has been preferred to glass because of the large size of the vessel needed. Furthermore, only metal is strong enough to enable the use of a rectangular cross section which takes best advantage of the limited volume of high and uniform magnetic field available. Copper has been preferred to stainless steel for this part of the cryostat, although it has less strength, because it has lower magnetic susceptibility and thermal properties favoring the persistance of isothermal conditions even in the absence of a fixed temperature bath. The weak points of a metallic Dewar are the presence of long welds: a leak is more likely to occur than in a glass vessel. The walls have not been silvered making its thermal characteristics less favorable. The heat-flow by conduction and radiation into the cold section of the cryostat is relatively large.

The inner Dewar contains the bath at the temperature to which we wish to bring the specimen. It is liquid helium, liquid nitrogen or DuPont freon 22. Other fixed points could be used without much complica-

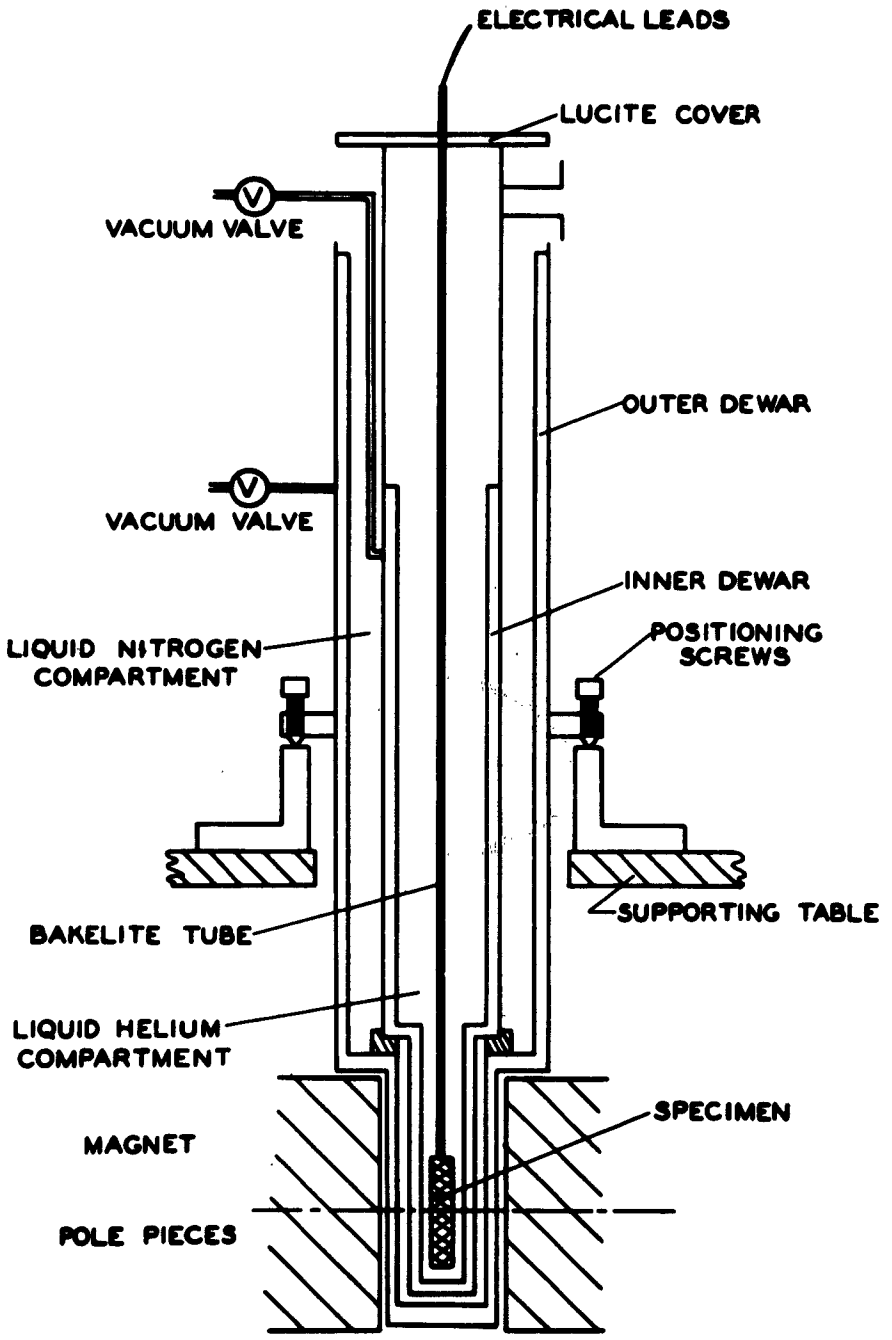

Fig. 12. Schematic diagram of the cryostat.

tion. When liquid helium is used, the space between the two vessels is filled with liquid nitrogen. Temperatures below 4.2°K could, in principle, be reached by partial evacuation of the inner Dewar, which can be completely closed by means of a lucite cover and an o-ring seal. Temperatures between the fixed points are obtained by letting the helium evaporate completely and the system warm up naturally until it reaches liquid nitrogen temperature. This temperature rise takes four hours and enables one to make several measurements with nearly uniform temperature of the specimen at any stage. After the liquid nitrogen in the outer Dewar has completely evaporated, the temperature rises again, slowly, up to room temperature. Thus any temperature between 4.2 and 295°K can be reached, but not maintained. The whole warm up process takes 18 to 24 hours. For a glass Dewar this period would be considerably longer. To prevent excessive condensation of moisture on the copper part of the Dewar, a 25 watt heating tape is wound around it, protecting the pole pieces against rust formation.

3.42 Considerations governing the design of the cryostat

The general shape of the cryostat and most of its dimensions are determined by its function, the size of the specimen, the dimension of the pole pieces and the air gap of the magnet. Only the thickness of the plates to be used has to be calculated. A compromise has to be realized between two conflicting factors. The plates have to be thick enough to stand the pressure, not to deform permanently and especially to prevent opposite walls from coming into contact by elastic deformation. On the other hand, if one wants to keep down the rate of heat inleak

through conduction by the walls, and also maintain open as large an inner cross-section as possible, the walls have to be of minimum thickness. The separation between opposite walls in a vacuum jacket should be large in order to keep down the heat transfer by radiation. Rather crude calculations can be carried out to determine the minimum thickness of the plates capable of standing a load of 15 psi. They are based on the elastic deformation of rectangular plates under uniform load with various boundary conditions[14]. Once the dimensions of the cryostat are all fixed, calculations are made to estimate the rate of heat transfer from the outside into the Dewar and obtain an order of magnitude of the rate of evaporation of the liquids used as coolants. A small fraction of this transfer takes place through conduction by the walls of the cryostat and the electrical leads (about 15 to 20%). Due to the large thermal gradients in the evacuated jackets of each Dewar, the largest part of the heat inleak occurs by radiation. The liquid helium, with a low heat of vaporization (900 calories per liter), boils off at the rate of about one liter per hour. Liquid nitrogen, which exchanges heat with the room directly and by a large area, receives much more heat, but, because of its higher heat of vaporization (40,000 cal/l), it evaporates only at 1.5 to 2 liters per hour.

3.43 Testing the cryostat

The good working conditions of the cryostat depend primarily on the quality of the vacuum realized and the length of time a good vacuum is kept. They can be checked in two different ways. A first test consists in following the pressure rise inside each of the vacuum shells by means of a type G.P. 140 Pirani Gauge (Consolidated Vacuum Co.), when the

whole system is at room temperature. Any value larger than 2 μ per hour, the normal rate of increase due to the outgasing of the walls, is an indication of a leak or some other defect. During the experiment itself, it is more convenient to consider the rate of boil off of the liquid helium and nitrogen. If the consumption of any of these two elements is significantly larger than the values estimated above, a defect might be present and should be located systematically using a leak detector. One has however to take into account an increase in helium consumption, due to the heat produced by very intense eddy currents set up in the part of the Dewar which is in contact with the liquid helium every time the magnetic field is reversed.

3.5 Temperature Determination

The temperature range covered is best separated into two intervals: above 20°K thermocouples can be used as thermometers, below 20°K methods using resistance or helium gas thermometers are more successful. In the present study a copper-constantan thermocouple was used jointly with carbon resistors. Both were calibrated over the entire temperature range of interest. This method was preferred to a more reliable platinum resistance thermometry, which cannot be used below 20°K. Furthermore only moderate accuracy is necessary for the present study.

3.51 Temperature measuring circuit

The circuitry for the measurement of the temperature in the cryostat is represented schematically in Fig. 13. There are actually two independent circuits, one using thermocouples, the other carbon resistors.

In a thermocouple, the temperature sensitive element is very small

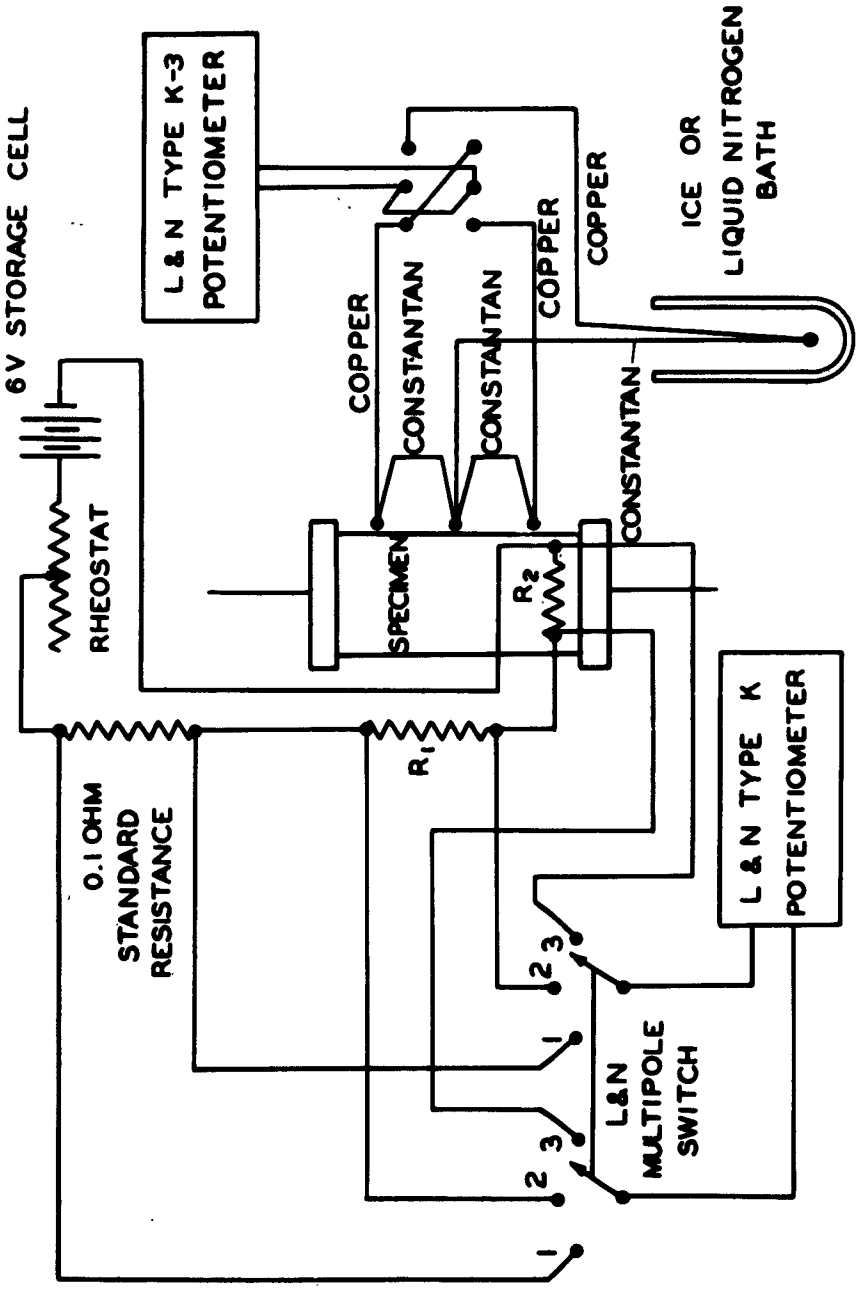

Fig. 13. Schematic diagram of the temperature measuring circuits.

and has quick response, making it possible to follow variations of temperature at a point. The simplest combination for low temperatures is copper against constantan. Its thermoelectric power is more favorable than that of other commonly used combinations. At the ice point it is 39 μV/°C; at 10°K it has dropped to 4μV/°C, which is still measurable. In the circuit shown there are three junctions: one is a reference junction placed in an isothermal bath of known temperature (liquid nitrogen or ice), the two others are located at both ends of the specimen holder. This arrangement enables the measurement of absolute temperatures as well as of longitudinal temperature differences along the specimen. Beaded junctions are obtained by heliarc welding. In the low temperature range, it is advantageous to use a reference junction at liquid nitrogen temperature in order to reduce the error due to this reference temperature. The thermal emfs are measured by means of the K-3 potentiometer within 0.5 μV. This sensitivity permits the use of thermocouples even at 4.2°K, where the thermoelectric power is very small. The impossibility of having the thermocouple juction in contact with the specimen may cause an error in the temperature determination, especially during the warm up period, where specimen holder and specimen may not be at the same temperature. However, because of the slow temperature rise and the presence of a large mass of copper surrounding the specimen assembly, this discrepancy is assumed small or comparable with the accuracy desired.

The circuit containing the carbon resistance thermometers was originally meant to cover the range from 4.2 to 50°K. Carbon or semiconducting materials have an increasing resistance with lowering tempera-

ture in opposition to metals like platinum, the resistance of which becomes much less temperature sensitive below 20°K. The resistance of the temperature sensitive elements is measured by the voltage drop across them when traversed by a small current (small to prevent heating of the resistors). The sensitive elements are homemade from ordinary radio resistors (a 10 ohm Allen Bradley and a 3.6 ohm Chmite resistor were used). The bakelite insulation is ground off and replaced by a thin baked-on coating of Glyptal varnish. Thus the element takes rapidly the temperature of the surroundings[15]. The advantage of carbon resistances over metallic ones is their much smaller change in presence of a magnetic field. The principal difficulty is to obtain reproducibility. Frequent recalibration is needed. Two such elements are used to enable the detection of eventual temperature inhomogeneities.

3.52 Calibrations

For the thermocouple, regular thermocouple wire was taken (Leeds and Northrup 24 B & S gauge, with insulation) for which the calibrations of 1921 and 1938 are valid. At several fixed points the measured and tabulated emfs were compared and the emf versus temperature curve for the actual thermocouple established. This curve was extended down to 4.2°K partly by continuity and partly by comparison with the indication of the carbon resistances. This method does not pretend to be very accurate.

Between liquid nitrogen and room temperatures, the indications of the thermocouple helped to determine the resistance versus temperature

curve of the carbon elements. A smooth curve was then drawn, joining this branch of the curve to the value at 4.2°K (Fig. 14). This procedure was preferred to an analytical determination of the coefficients of the theoretical relation,

$$\ln R + \frac{k}{\ln R} = A + \frac{B}{T}$$

The number of data did not justify a least squares determination of A, B and k. The curves of Fig. 14 helped then to draw the low temperature portion of the thermocouple calibration curve (Fig. 15). This procedure is good enough since an uncertainty of ± 1°C in T is considered tolerable. However, readings on the potentiometer are far more accurate and with an exact calibration of the thermocouple, the temperature could be read within hundredths of a degree, even below 20°K.

Periodic checks at room temperature, 4.2 and 77.4°K of the indications of thermocouples and carbon resistors showed a satisfactory stability of both instruments under the conditions of the experiment (repeated thermal cycling).

In practice, once the thermocouple had been calibrated over the whole range of interest, it was used alone, because it is much more convenient. Furthermore, it is more likely to give an instantaneous temperature, not too far from the actual temperature of the specimen, whereas the carbon resistors take much longer to reach the temperature of the surroundings. During the warm up period, an average temperature was assigned to each measurement by taking the mean of the temperature read just before and just after the actual measurements.

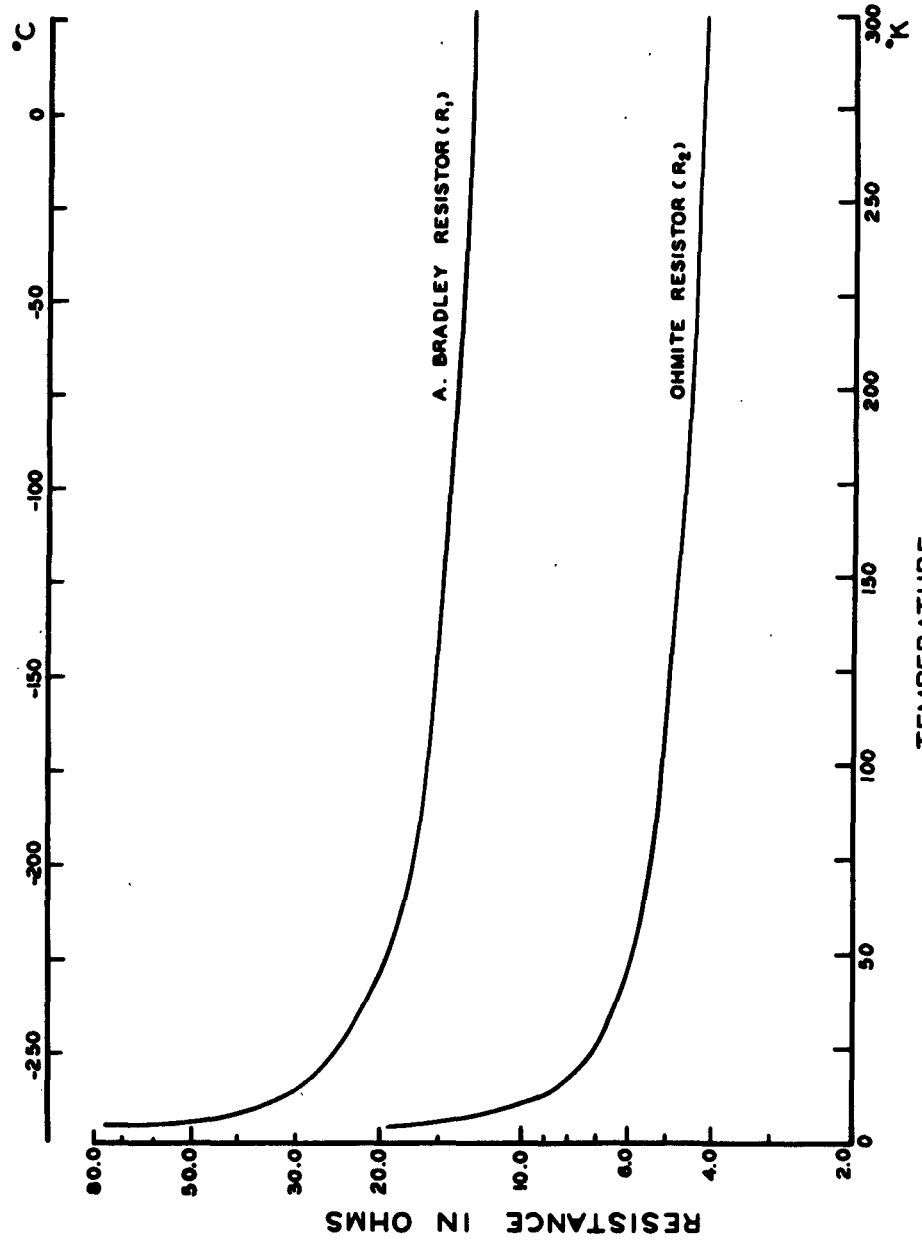

Fig. 14. Calibration curves of the two carbon resistance thermometers.

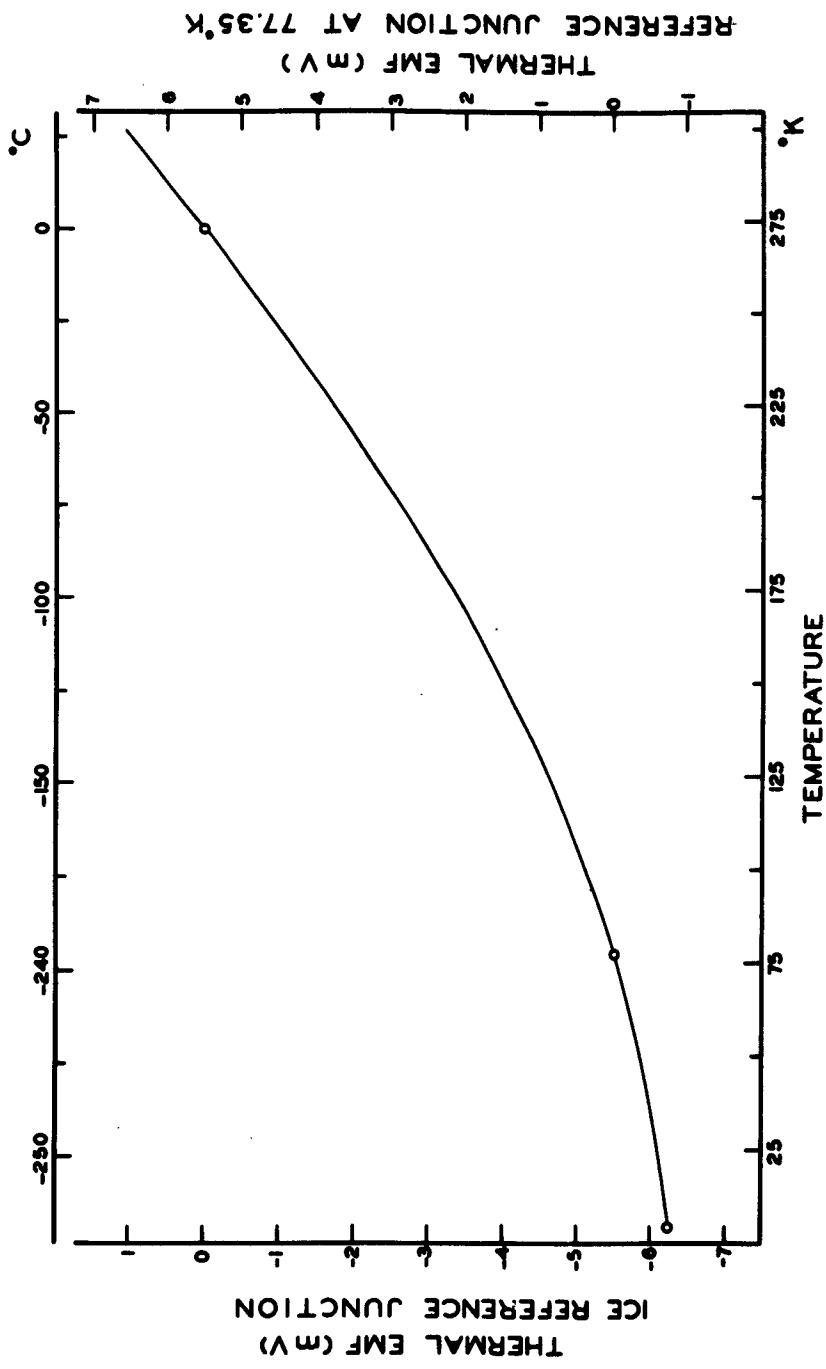

Fig. 15. Calibration curve of the copper-constantan thermocouple.

3.6 Operating Procedure and Calculation Methods

Before each test, both shells of the cryostat are evacuated by means of a mechanical vacuum pump to about 40 microns of mercury. The power supply and the amplifier are turned on. The inner Dewar is cooled down to 77.4°K by pouring just enough liquid nitrogen into it. The outer Dewar is then filled with liquid nitrogen and an atmosphere of helium is maintained in the inner Dewar, completely isolated from the atmosphere. Sufficient time is given for the whole system to reach steady state conditions at that temperature. The current through the specimen is turned on and the Helipot adjusted, such as to minimize the voltage between A and B. The magnet power supply and the cooling water are then turned on and liquid helium is transferred into the inner Dewar, until its level is well above the specimen. The operation requires a total amount of helium of nearly 10 liters. The magnetic field is adjusted to its desired value and measurements can be started.

3.61 Resistivity measurements

The resistivity can be computed from the experimental determination of the current, the voltage drop V_{CD} and the temperature. Current and temperature are taken as the average of readings taken just before and just after the measurement of V_{CD}. In this manner variations of these quantities over the time of a measurement are taken into account (drift in the power supply, of the temperature, gradual change in the resistance of the circuit). The result of this measurement is a resistance R_{CD}, easily convertible into resistivity.

$$\rho = \frac{V_{CD}}{I} \times \frac{tb}{l} = k_1 \frac{\Delta V}{I} \text{ , } (\Delta V = V_{CD})$$

k_1 is a geometrical factor depending on the dimensions of the specimen and the distance between the probes C and D. In this formula, an average value has been obtained for the thickness t from the weight of the sample. Since this measurement is made in presence of a magnetic field, ρ contains magnetoresistance. However, the error thus introduced is negligible[16]:

$$\frac{\Delta\rho}{\rho} = B_t H^2 \simeq 6.6 \times 10^{-13} \quad H^2 \simeq 4 \times 10^{-5} \text{ when H = 8 kilogauss.}$$

This is smaller than the experimental uncertainty.

3.62 The Hall voltage

In presence of a magnetic field the voltage between A and B can be written

$$V_{AB}(B) = V_o + V_1(J) + R_H BJ$$

B is the magnetic induction, J the current density. $V_1(J)$ is a small voltage, depending on J, due to the imperfect alignment of probes A and B and the anisotropy of the resistivity tensor. R_H is the Hall coefficient and V_o is a spurious voltage including thermals in the measuring circuit, pick up from the building, various thermomagnetic and galvanomagnetic contributions. The voltages included in V_o can be separated into those which are constant or time dependant, those which reverse with J, or B, or J and B, those which depend or do not depend on B. No measuring technique can eliminate them all, nor even separate them from the Hall voltage. V_o is found to fluctuate in an unpredictable manner and with no apparent periodicity. Its magnitude increases with temperature

and makes Hall measurements more difficult. Because of the presence of V_o, the full accuracy of the amplifier had to be sacrificed to a more rapid method in which fluctuations in V_o have less effect: the fractional part ($< 10^{-7}$ volt) of the voltage was estimated visually from the deflection on the galvanometer scale. Furthermore each measurement had to be repeated several times and averaged to eliminate as much as possible the random fluctuations. Due to the limiting values at temperatures below 77°K of electrical and thermal properties of the materials used, V_o was very small and had no widely fluctuating part in that range of temperatures. Resonable accuracy was then possible in the determination of $V_{AB}(B)$. The Hall voltage is obtained as an average over three measurements of V_{AB}: with the magnetic field in one direction ($V_{AB}^{(1)}$), then in opposite direction ($V_{AB}^{(2)}$), and then back to the initial direction ($V_{AB}^{(3)}$).

$$V_H = \frac{1}{4}\left[V_{AB}^{(1)}(B) + V_{AB}^{(3)}(B) - 2\,V_{AB}^{(2)}(-B)\right]$$

This procedure eliminates V_1 as well as those parts of V_o which do not reverse with the magnetic field. It does not get rid, however, of the fluctuating part of V_o and some of the thermomagnetic effects. Reversal of the current eliminates most of the latter, whereas the effect of the fluctuations cannot be compensated for. Above liquid nitrogen temperature, where they become important (comparable in magnitude to the Hall voltage), the Hall voltage can no longer be measured, unless V_o is considerably reduced by putting the specimen into an isothermal bath.

At fixed points, where the temperature can be maintained constant

over a longer period of time, the magnetic field dependence of V_H has been investigated by varying B from 3 to 9 kilogauss. If V_H is not proportional to B, all measurements have to be made with the same magnetic field.

From the Hall voltage, the Hall coefficient itself is derived by the following formula:

$$R_H(T) = V_H \times \frac{t}{B\,I} = k_2 \times \frac{V_H}{I}$$

3.7 Accuracy and Limitations

There are two different categories of uncertainties involved in the determination of resistivity and Hall coefficient. First, the errors in the determination of B, ℓ, t, b introduce an uncertainty in the numerical factors k_1 and k_2. They are the same for all experimental determinations on a given specimen. On the other hand each individual measurement of V_H or ΔV involves errors varying with each experimental point.

3.71 Resistivity

The larger part of the uncertainty in the resistivity values comes from the numerical factor $k_1 = tb/\ell$. The dimensions b and ℓ are several centimeters and are known within 1%. The width b of the plate can be considered constant within the same factor. The value of t is obtained indirectly and has a relative uncertainty of about 1.5%, most of it due to the dimensions, not the mass. k_1 has then associated with it an uncertainty of nearly 4%.

On the other hand, ΔV is read on the K-3 potentiometer with 0.5 μV and I is given by the type K potentiometer with four significant figures.

However, the drift of the constant current supply reduces the precision in I to 0.1%. The resistance R_{CD} is therefore measured at ± 0.2% (magnetoresistance changes are 4×10^{-5}). Another important source of error in the resistivity versus temperature curves arises from the uncertainties in the temperature measurements. Not only may the temperature not be uniform over the entire specimen, but it may also be different from the temperature recorded by the thermocouple. In unfavorable cases, the differential thermocouple registered a 1°C temperature difference between top and bottom of the specimen. This is of the same magnitude as the uncertainty in the low temperature part of the calibration curve. One can therefore not expect to know T to better than ± .5 or ± 1°.

3.72 Hall coefficient

The uncertainty in the Hall coefficient has a threefold origin. The major source of error is introduced by the measuring technique itself. What has been chosen in section 3.62 to represent the Hall voltage contains, in fact, several small transverse effects, negligible only if perfectly isothermal conditions are set up, i.e., at a very few fixed points. Due to the misalignment of the probes, part of the longitudinal effects is measured together with the Hall effect. A systematic error is introduced if the specimen is not perfectly normal to the magnetic field lines. Thanks to the use of titanium leads and an averaging procedure, the resulting error in V_H should not exceed 3%.

In the second place, there is the uncertainty in the conversion factor $k_2 = {}^t/B$. The magnetic field, 8 or 9 kilogauss usually, is determined from the logging scale of the NMR fluxmeter within ± 10 gauss or

0.1%. The homogeneity of the field over the region of the specimen is better than this value. As far as t is concerned, its average value is determined to 1.5%, but its lack of uniformity causes a perturbation on V_H, which cannot be numerically estimated and which is not completely compensated for by taking an average value. Nevertheless, the uncertainty in k_2 should not be greater than 2%.

Finally, uncertainties are introduced by the measurement of V_H and I. The current is measured in the same way as for resistivity calculations. Its relative uncertainty is .1% and can be neglected in comparison with the scatter and uncertainty in the Hall voltage. The noise V_o, always present in the observation of V_H, becomes increasingly troublesome as the temperature is raised, requiring several measurements to be taken and averaged and the time between measurements with reversal of the magnetic field to be kept as short as possible. This difficulty is the major drawback of the method and leads to an uncertainty in V_H which can reach 8% or more (a typical measured voltage is then .30 μV ± .02 μV).

The combined effect of all these sources of error leads to an experimental uncertainty in the Hall coefficient of 5 to 10%. The accuracy is better below 77°K where V_o is small and steady. Above 77°K reliable values can only be obtained when the specimen is placed in an isothermal environment with controlled temperature. This difficulty reduces the chances of finding a general quantitative interpretation of the results.

4. SPECIMENS

4.1 Origin and Preparation

The specimens used in this investigation were made from a piece of iodide titanium, about 5x4x0.4 cm, cut from a strip of hot rolled, remelted titanium. The material was obtained from the U. S. Army Ordnance Corps, Watertown Arsenal Laboratories. Part of the same plate has been used previously for accurate lattice parameter determination as a function of temperature[17]. The piece of metal was milled on both sides in order to remove the contaminated layers developed during previous operations.

No quantitative chemical nor spectroscopic analysis of the material was available. However the iodide process leads to very pure titanium. This is confirmed, on the one hand, by the measured values of the lattice parameters, and on the other hand, by the ratio of the resistances at room temperature and liquid helium temperature, which was quite high (around 30).

The piece of titanium of initial thickness of about 4 mm was first cold rolled into a strip 0.02 cm thick. After this 95% reduction, part of the sheet was kept to that dimension, whereas the rest of it was reduced further to a final thickness of 0.008 cm. Specien No. 1 was made out of that sheet. However, before measurements could be made, a stress relief treatment had to be performed. The specimen was heated for one hour at 500°C. Since titanium is a very reactive metal, the specimen was first cleaned in an acid etch of equal parts of nitric acid, hydrofluoric acid and glycerin. This insured that impurities, contained in the surface layers and coming from the rolling mill or superficial oxidation, were removed and prevented from diffusing into the interior of the specimen during the subse-

quent heat treatment. The specimen was sealed in a pyrex tube filled with purified helium. Care was taken to insure that the specimen did not touch the pyrex by being clamped between two larger sheets of titanium. This procedure had the further advantage of straightening the specimen, which was no longer perfectly flat after the cold rolling. A "getter" was heated inside the tube to capture the remaining traces of oxygen and nitrogen prior to the treatment. After the treatment, the specimen was quickly returned to room temperature. It was then cut to the final dimensions with straight and parallel edges. A back reflection pinhole diffraction pattern with copper K_α radiation was taken on a fraction of the specimen and compared with a similar pattern made prior to the heat treatment. The broad diffuse Debye ring had been replaced by two much sharper and well resolved rings corresponding to the K_α doublet, proving the effectiveness of the treatment.

The two other specimens were obtained from the remaining part of sheet that had received only a 95% reduction. This sheet was treated for stress relief before any further reduction in the way just described for specimen 1. Then a piece of about 12 cm long was cut out of it and cold rolled in the transverse direction, in order to produce a different texture. However, the thickness could only be reduced from 0.2 mm to 0.1 mm. This specimen was sealed in a pyrex tube and treated for one hour at 500°C with the precautions already mentioned. The result was specimen No. 2. After all measurements on it were completed and a piece saved for x-ray investigation, specimen 2 was annealed in order to produce a third texture. For this purpose, it was enclosed in a quartz tube with a titanium getter and rested only on titanium supports away from the quartz walls. The specimen

was heated for one hour at 950°C. It was then brought back to room temperature. This recrystallized sample was designated specimen No. 3.

Before mounting each specimen for Hall measurements, the dimensions were measured, in particular the average thickness. A check with a micrometer revealed that, at least for specimen 1, the thickness varied appreciably about the mean value. This is a consequence of the chemical etch: the lead dish in which the operation was carried out, was too small to enable the etching of the whole specimen at the same time.

4.2 Principle of Texture Determination

In order to interpret the results of the Hall coefficient determination and in particular to relate them to the intrinsic galvanomagnetic coefficients $R_{\parallel}$ and $R_{\perp}$, the knowledge of the texture of each specimen is required, i.e., the orientation of the grains in the polycrystalline sample and the relative importance of each particular orientation. The interest of highly textured specimens, where one particular grain orientation is predominant, is that such specimens reflect to a greater or lesser degree the properties of a single crystal. Rough calculations can be carried out by replacing the specimen by a single crystal having the mean orientation of the grains of the polycrystalline sample. Deformation and recrystallization textures, as are obtained in the present case, usually fall into this category. A directional character due to preferred orientation is therefore expected in most properties which depend on crystallographic direction in single crystals.

Preferred orientation is best described by means of a pole figure. This is a stereographic projection which shows the location and density of

poles of a specific crystallographic plane. For sheet specimens, the plane of the stereographic projection is parallel to the plane of the sheet and the longitudinal direction of the sample (in most cases the rolling direction) is indicated on the perimeter of the basic circle (equator) of the pole figure. However, since a large number of crystals must be considered to obtain a representative picture of the texture, instead of individual poles being plotted, equidistant contours are used to represent the average population of poles at all positions about the sample. A perfectly random polycrystalline sample has poles uniformly distributed over the reference sphere, but not on the projection, which is not area-true. In a textured specimen, poles cluster in certain areas of the pole figure.

The techniques used to determine the pole figures in this investigation use x-ray diffraction and are described next.

4.21 Photographic method[18]

X-ray methods of determining pole figures use the fact that x-ray diffraction averages automatically the contributions from many grains, provided the grain size is not too large. The (hkl) pole figure is constructed by analyzing the distribution of intensity around the circumference of the (hkl) Debye ring, since the observable spatial distribution of x-ray diffraction intensity is identical, within a proportionality factor, to the density of poles on a reference sphere centered at the specimen.

In the film technique, a series of transmission pinhole photographs are taken with the sheet first normal to the incident beam, then inclined at an angle η about either the transverse or the longitudinal directions. The blackening of the Debye ring of interest is observed as a function of

the angle λ (Fig. 16) and plotted stereographically, using the rather complicated method described in reference 18 (page 282). By successive changes of η the whole pole figure can be covered. Two important disadvantages of this method are the inaccuracy in visual intensity evaluations and the necessity of a different geometrical net for each specimen examined. Thus only qualitative pole figures are obtained. But they are often sufficient to give information about an "ideal" or predominant orientation and the degree of scatter about it.

A more quantitative pole figure is obtained by "reading" the photographic film with a microphotometer and plotting isointensity contours. However an absorption correction has to be applied, to take into account the variation with η and λ of irradiated volume and path length of the x-rays. This correction is given by the following formula[19]:

$$\frac{I(\eta,\lambda)}{I(0)} = \frac{k}{k_o} \exp\left\{ - \left[k(1+a) - k_o(1+a_o) \right] \right\} \frac{\sinh k(1-a)}{k(1-a)}$$

in which $k = \frac{k_o}{\cos\eta} = \frac{t\mu}{2\cos\eta}$, μ is the absorption coefficient of titanium,

$$a_o = \frac{1}{\cos 2\theta} \quad , \quad \frac{1}{a} = \cos 2\theta + \sin 2\theta \tan\eta \cos\lambda \ ,$$

and θ is the Bragg angle.

This factor has been plotted on Fig. 17 for the $(10\bar{1}0)$ reflection of specimen 1. Another inconvenience of the photographic method appears now: the absorption correction depends on two parameters and a similar set of curves has to be computed for each specimen and each reflection. In the diffractometer method, the correction factor varies with only one angle.

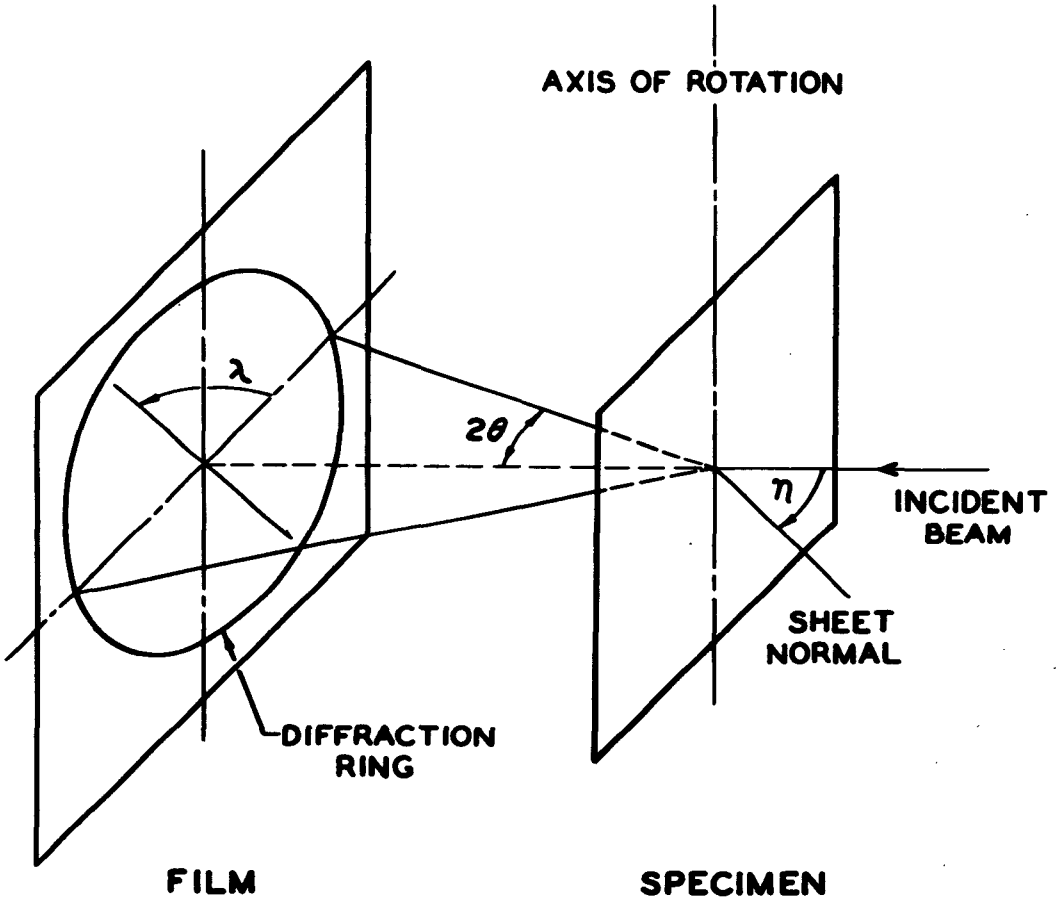

Fig. 16. Transmission method for pole figure determination (film technique).

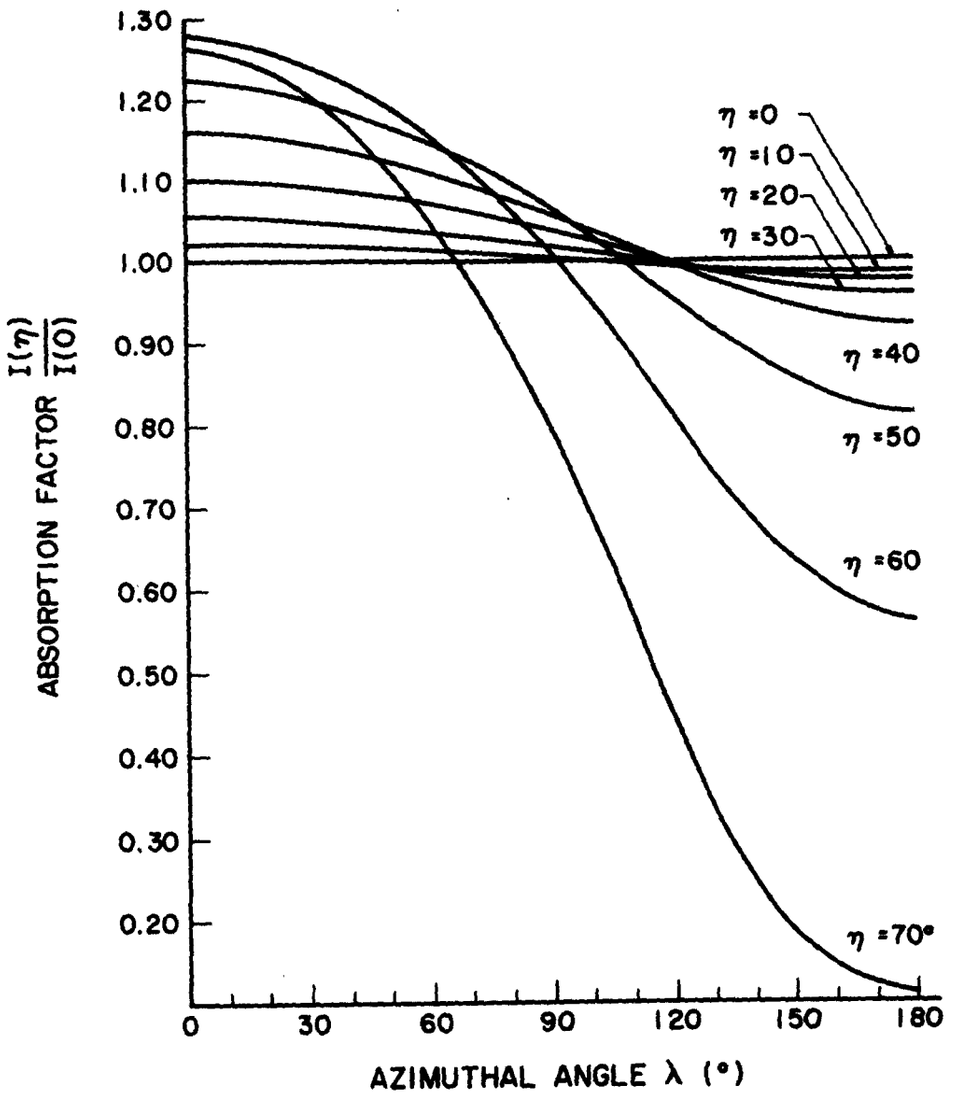

Fig. 17. Absorption correction factor for specimen No. 1 and the (10$\bar{1}$0) reflection (MoK radiation).

Intensities observed on different films are made comparable by examining a reference pattern of a fine powder of anatase (TiO_2) taken and processed under the same conditions as the main pattern. Thus variations in exposure time and processing can be taken into account.

4.22 Diffractometer method

A faster and more quantitative technique for pole figure determination is the one originally proposed by Decker, Asp and Harker[20]. It uses a radiation counter associated with an x-ray diffractometer (of vertical axis in the present case). X-rays striking the specimen are diffracted to a stationary counter, set at the proper 2θ angle for the crystallographic plane chosen. The specimen holder allows rotation of the specimen about the diffractometer axis and about a horizontal axis normal to the specimen surface. In order to explore the complete Debye ring, the specimen has to be rotated about the second axis. The angle of this rotation, β, is measured clockwise and indicates the amount by which the transverse direction is rotated about the sheet normal, out of the horizontal plane, and is zero when the transverse direction is horizontal (Fig. 18). The angle between the sheet normal and the normal to the plane, reflecting into the counter is denoted $90° - \alpha$. For a given position of the specimen, the normal to the planes which diffract x-rays towards the counter can be defined by the two polar angles α and β with respect to the xyz axes: α is the latitude and β the longitude or azimuth counted from the transverse direction (Oy). Because of the symmetry planes of the textures (the three coordinate planes defined by the xyz axes), the sign of α and β does not matter. $\alpha = 0$ corresponds to planes perpendicular to the sheet and $\alpha = 90°$ to planes

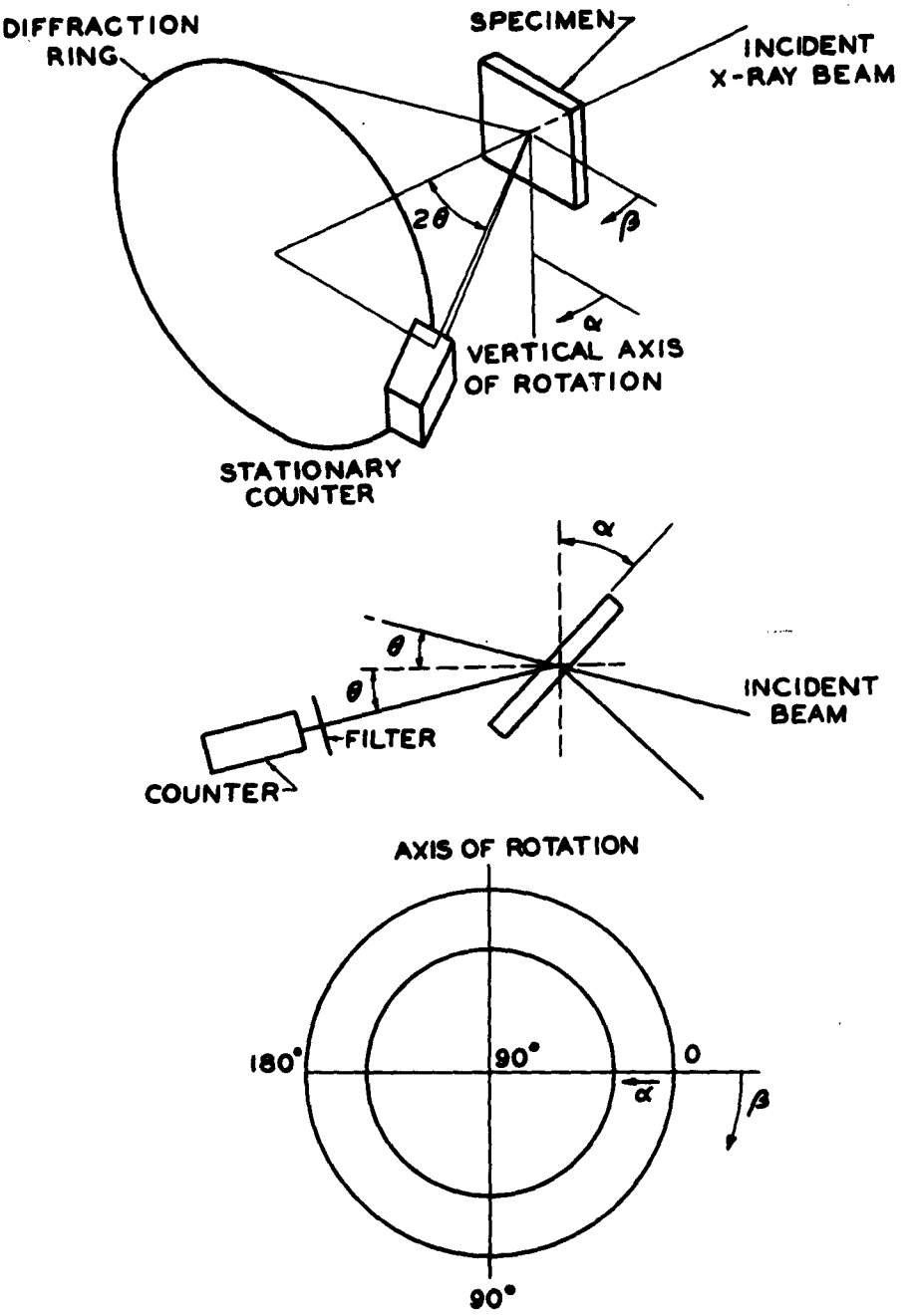

Fig. 18. Principle of pole figure determination by the diffractometer method (transmission).

parallel to it. On the stereographic projection β is measured counterclockwise around the pole figure and α is measured radially from the equator towards the center of the projection. In order to cover the whole area of the pole figure, the specimen has to be studied both in transmission and reflection[21]. In transmission, the specimen may diffract to the counter when set at any β angle, whereas the α angle is limited to $90^\circ - \theta$. The central part of the pole figure is determined by reflection. The counter is set at a new angular position $2\theta'$, where it will receive a higher order reflection from the same set of planes (hkl); θ' is larger than θ. The specimen is initially set so that it bisects the angle between incident and diffracted beams ($\alpha = 90^\circ$). In the reflection method, α can be varied from 90° to $90^\circ - \theta'$. This way there is always a range of α angles where data obtained by transmission overlaps that obtained by reflection. This is not only a check, but it also allows to establish the correspondance between the intensity scales used in the transmission and back reflection regions. For a given position of the specimen, described by the angles α and β, the measured intensity, after correction for absorption, gives a number which is proportional to the pole density at the corresponding point of the stereographic projection. When a polar stereographic net is used, the plotting of the data is therefore straightforward.

Two corrections have to be applied to the measured intensities before they are plotted onto the pole figure. There is first an absorption correction, because variations in α cause variations in both the volume of diffracting material and the path length of the x-rays within the specimen. Variations in β have no effect. The equations which apply to the conditions

described above are:

- for transmission[22]

$$\frac{I(0)}{I(\alpha)} = \frac{\mu t}{\cos\theta} \exp\left[-\frac{\mu t}{\cos\theta}\right] \frac{\left[\cos(\theta-\alpha)/\cos(\theta+\alpha)\right]-1}{\exp\left[-\mu t/\cos(\theta-\alpha)\right] - \exp\left[-\mu t/\cos(\theta+\alpha)\right]}$$

- for back reflection[23]

$$\frac{I(0)}{I(\alpha)} = \frac{\mu t}{\cos\theta}\left[1-\frac{\cos(\theta+\alpha)}{\cos(\theta-\alpha)}\right] \frac{\exp\left[-\mu t/\cos\theta\right]}{1-\exp\left[\mu t/\cos(\alpha+\theta) - \mu t/\cos(\alpha-\theta)\right]}$$

The absorption factor $I(\alpha)/I(0)$ has been plotted on Fig. 19 for the transmission method in the case of the $(10\bar{1}0)$ pole figure of the three titanium specimens investigated, when molybdenum K_α radiation is used. The intensity entering in these formulas is the integrated intensity of the diffracted beam. The calculated correction factor is therefore meaningful only if the x-ray beam is not too divergent, so that it is received entirely by the counter.

The second correction consists in subtracting the background from the total intensity, because it contains contributions which are not proportional to the density of poles. The background is measured by slowly scanning over the diffraction peak and noting the counting rate just before and just after the peak. The operation is repeated for each setting of α. The background intensity is assumed independent of β and is best measured by replacing the actual specimen by a texture free sample of the same μt. This random sample can also be used to measure the maximum peak intensity at various α settings. The intensities from the textured specimen can then be expressed in multiplicities of these values corrected for background. This procedure saves the trouble of computing the absorption correction, since it is automatically

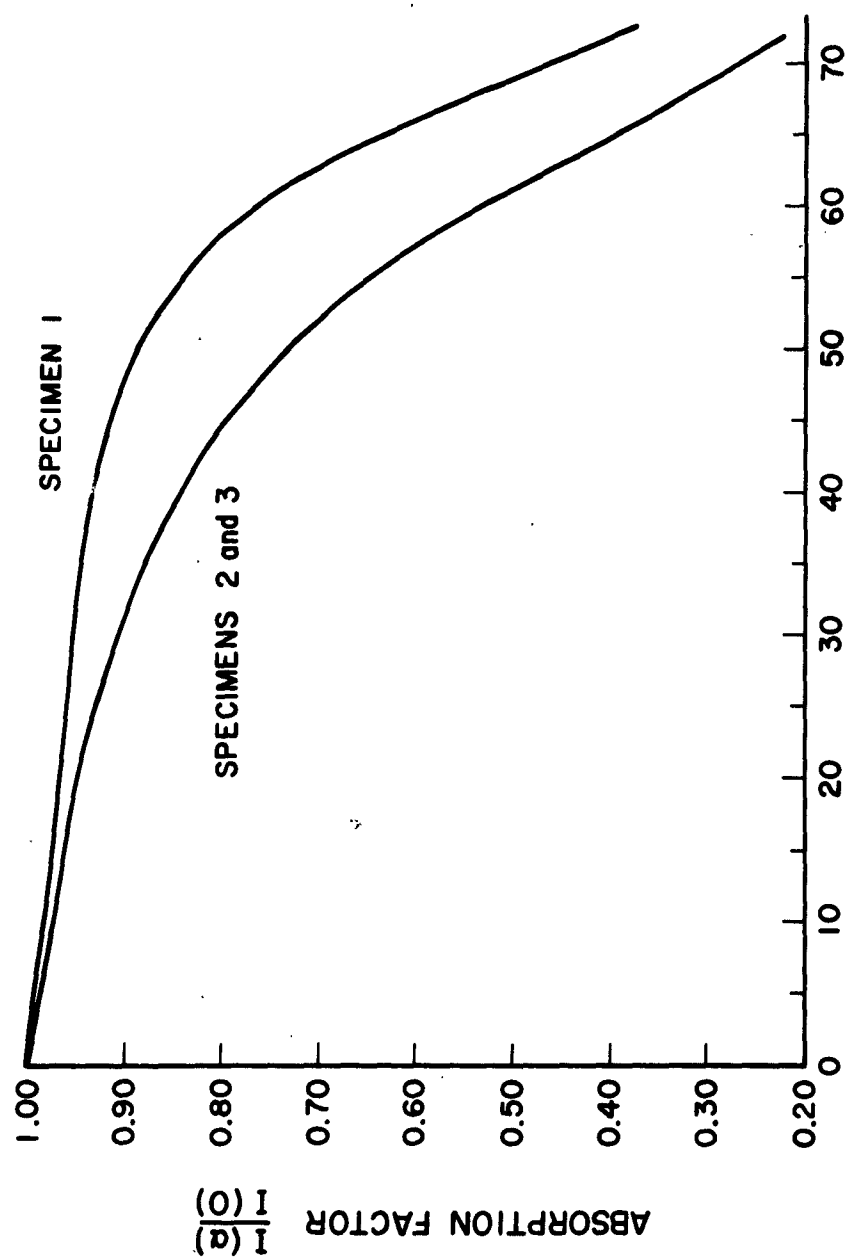

Fig. 19. Diffractometer method. Absorption correction in transmission.

included by the choice of the standard intensity levels.

The equipment used in the performance of this experiment is a General Electric XRD 5 diffractometer equipped with a proportional counter. The specimen is mounted on an automatic integrating pole figure goniometer (Model A 4968B) which allows both the α and β roatations. The specimen is held against a thin ring which rotates slowly in its own plane, thereby varying the angle β . In addition the specimen holder oscillates in a vertical direction at the rate of one stroke per second with an amplitude of one inch. Thus the intensity from a large number of grains is averaged, even for the larger grain size of recrystallization textures. At each vertical stroke the ring is advanced about 15 minutes of arc (every 2 seconds). While the β rotation and the vertical translation take place, the α setting remains constant until the complete circumference of the Debye ring is described. Then the specimen holder is automatically rotated by 5° about the diffractometer axis corresponding to a 5° advance of the angle α . The intensity detected by the proportional counter is fed into a pulse height analyzer (Nuclear-Chicago model 1810 radiation analyzer) which lets only radiation near the characteristic wavelength chosen go through. Its output goes to a Beckman Universal E-put and Timer, Model 7360. This instrument is set so as to count x-ray pulses for 10 seconds. The total number of counts is then printed on paper tape by a Berkeley model 1452 digital recorder. The counting and printing cycle takes nearly 11 seconds but starts only at even seconds. Each number on the tape corresponds then to a range in β of about 1.5° of arc. An exact correlation between numbers on the tape and the value of β can easily be established. Furthermore every time α

changes by 5°, a coded signal is printed on the paper strip. This method produces information in numerical form, which is easier to work with than chart recordings.

Errors in the interpretation of a pole figure can arise because of the presence of spurious intensity maxima. First there might be a second set of planes, (h'k'l'), with nearly the same spacing than the (hkl) planes. There is a possibility that the counter, set to receive one reflection, gets also part of the second peak because of a too wide receiving slit or an excessive divergence of the x-ray beam. A proper choice of slits, made after the diffraction pattern in the neighborhood of the peak of interest has been explored, reduces considerably the chances of an error of that type. In the second place, there might be a set of planes, (h"k"l"), and a strong component in the white radiation of the tube for which the Bragg angle is almost equal to the Bragg angle θ of the (hkl) planes with the K_α radiation. Misleading maxima appear then when the orientation of the sample is such that the (hkl) planes contribute little, but the (h"k"l") planes much, to the diffracted intensity. This cause of error can be eliminated in many cases by filtering the radiation and making a pulse height analysis of the pulses coming from the proportional counter.

4.3 Texture of the Three Specimens

4.31 Experimental details and procedure

Each specimen was studied by both methods. In the photographic method molybdenum K_α radiation was taken. A zirconium filter eliminated most of the β component (the (0002) and (10$\bar{1}$1) maxima from K_β coincide almost with the (10$\bar{1}$0) maximum from K_α) and reduced considerably the components in the

continuum the intensity of which is high in the primary x-ray beam. Exposures of 3 or 4 hours were made. η was varied in steps of 10° from 0 to 70°. The photographic method could not be applied to the third specimen, which had too large a grain size and could not be translated back and forth in the x-ray beam. A qualitative and rather crude pole figure of the $(10\bar{1}0)$ planes was made in each case and used as basis of comparison with the more detailed pole figure obtained by the diffractometer, in view of detecting possible spurious maxima in the latter pole figure. Furthermore the films showed clear, well defined rings and no streaks nor dark areas due to diffraction of white radiation. The results of the diffractometer method can therefore be used with confidence.

Although the pole figure of most interest in this study concerns the (0002) planes, the $(10\bar{1}0)$ reflection was preferred because this line is better separated from adjacent peaks and the corresponding pole figure is still easy to interpret. In the diffractometer method, molybdenum K_α radiation was preferred to copper, in transmission, because of its higher penetrating power and because it produces less fluorescence in the specimen. A 1° divergent beam has been adopted so that a fairly large number of grains are irradiated simultaneously. No receiving slit is used in front of the counter window, which has beenan aperture of nearly 1° and can receive the whole $(10\bar{1}0)$ peak but no appreciable contributions from the adjacent (0002) peak. Thus the counting rate will not be affected by a possible change in the shape of the peak when α is varied. Wavelengths other than MoK_α are prevented from reaching the counting unit by a zirconium filter and by the pulse height analyzer.

X-rays of wavelengths greater than the zirconium absorption edge and not eliminated by the radiation analyzer, will not contribute much to the diffracted intensity, because they correspond to weak components in the spectrum of the incident beam. For the back reflection region, copper radiation and the $(20\bar{2}0)$ planes were chosen because the corresponding angle θ' was large and allowed a larger range of variation for α (about 40°). However no useful information could be obtained, on account of a poor peak to background ratio and too small a density of poles in that region of the pole figure. The range $70 < \alpha \leq 90°$ of the pole figures has thus not been determined. This is no handicap, because the transmission data alone determine the texture without ambiguity.

Background corrections are obtained experimentally as described earlier. The correction for absorption is computed from the average thickness and the tabulated mass absorption coefficient, although an experimental measurement of μt would have been preferable. A comparison with a random sample has not been estimated useful. Isointensity contours drawn in arbitrary units, but equally spaced, give a representation of the texture significant enough for our purpose.

4.32 Results of the texture investigation

The pole figures of specimens 1, 2 and 3 are reproduced in Fig. 20, Fig. 21 and Fig. 22.

Although the pole figure itself is the best description of the texture, it will be convenient to represent it by an ideal orientation, i.e., the orientation of a single crystal whose poles lie in the high density regions of the pole figure. This will simplify the interpretation of the

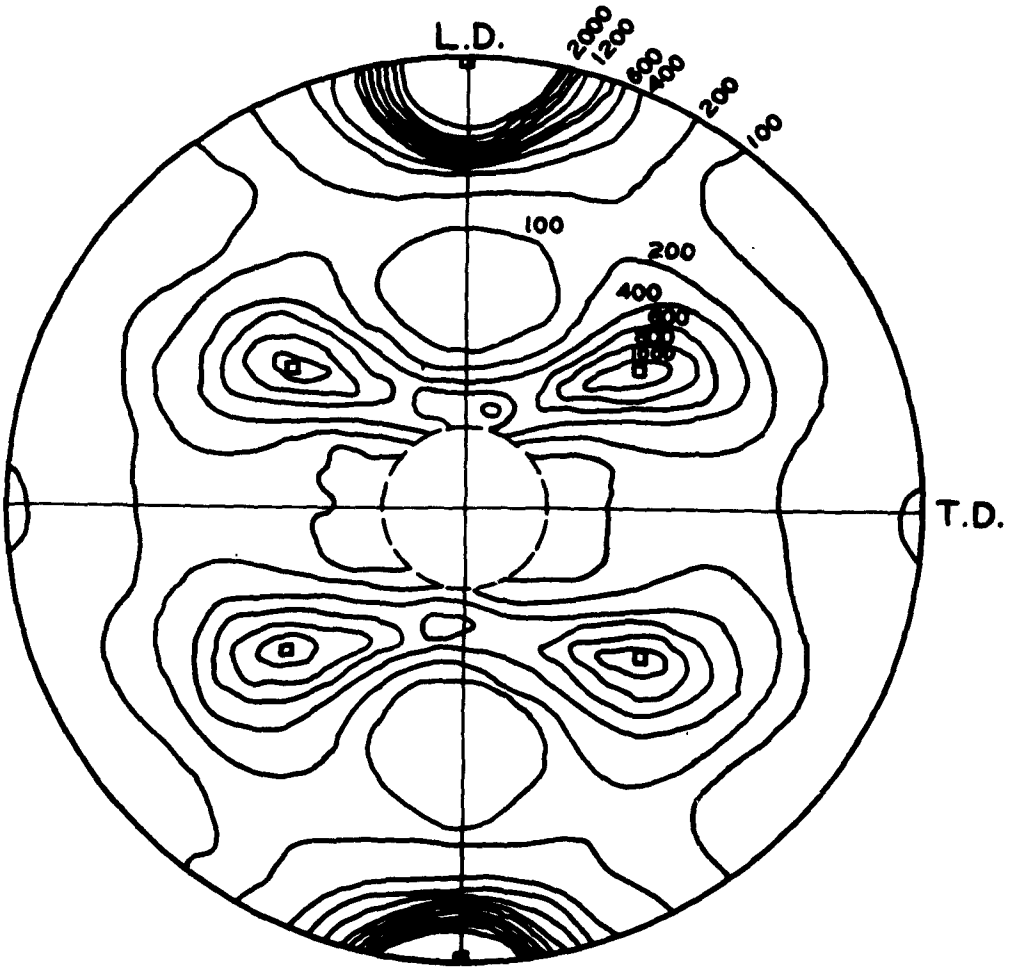

Fig. 20. $(10\bar{1}0)$ pole figure of specimen No. 1. The mean orientation is indicated by little squares. Isointensity contours are equally spaced (200 in arbitrary units).

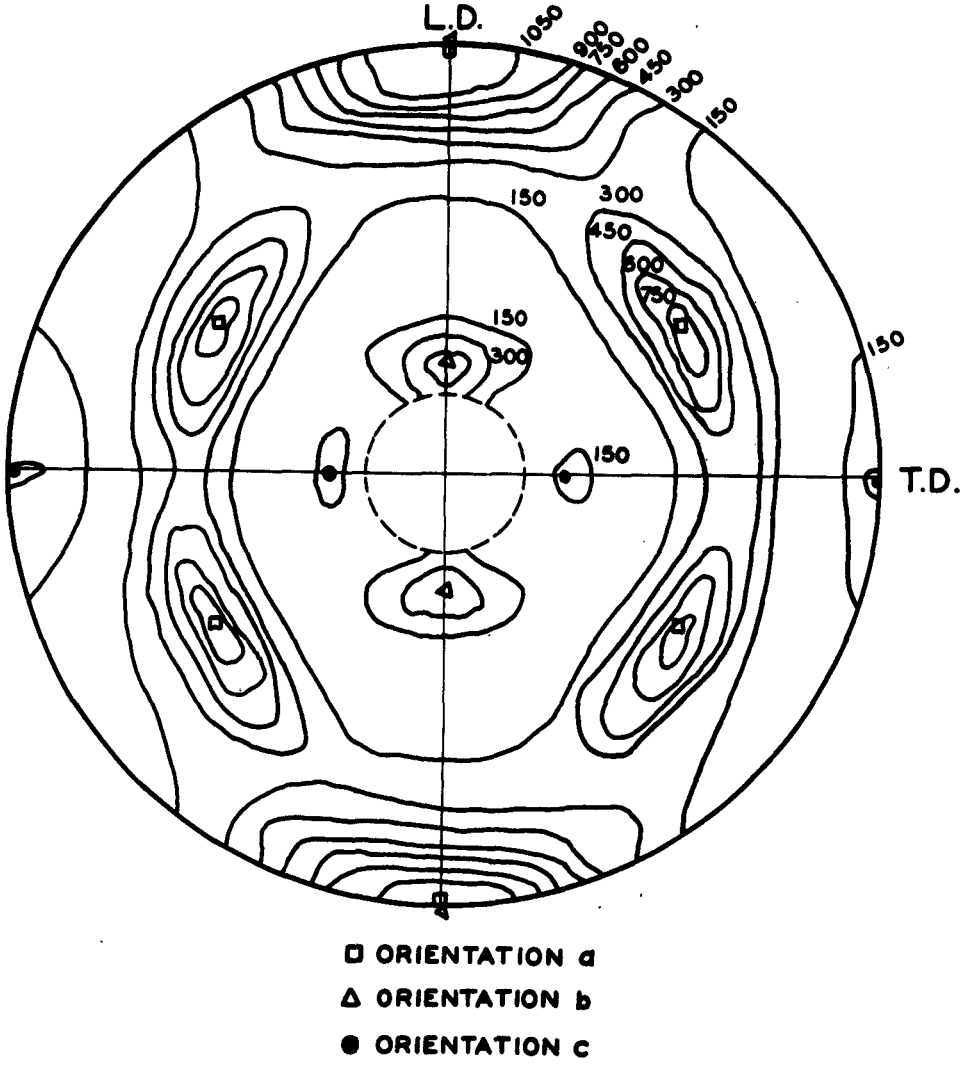

Fig. 21. (10$\bar{1}$0) pole figure of specimen No. 2 with indications of the predominant orientations. Isointensity contours are equally spaced (150 in arbitrary units).

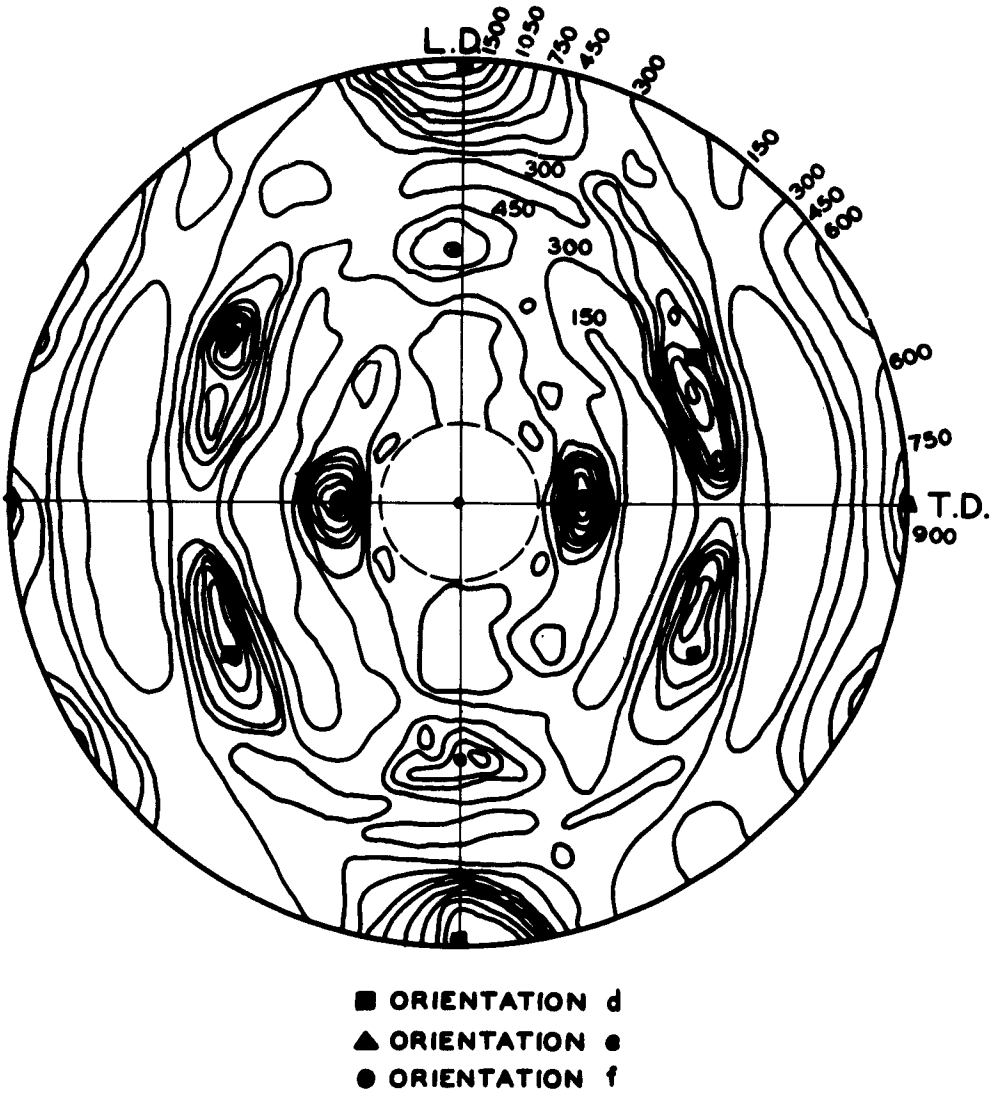

Fig. 22. (10$\bar{1}$0) pole figure of specimen No. 3 showing three predominant orientations. Isointensity contours are equally spaced (150 in arbitrary units).

experimental results in a later section.

There are six areas of high density of poles in the stereographic projection corresponding to specimen 1. The center os these areas, indicated by little squares, represent the poles of six equivalent $(10\bar{1}0)$ faces of the hexagonal prism of a single crystal with the following orientation: the $[10\bar{1}0]$ direction is parallel to the longitudinal direction (the x axis); the hexagonal unit cell is tilted in such a manner that the basal planes are rotated $45\pm2^\circ$ out of the rolling plane about the rolling direction. There are two equivalent orientations defined by these angles; they are mirror images of one another with respect to the plane of the sheet.

The pole figure of specimen 2 looks similar to the previous one. There is a large amount of preferred orientation: the $[10\bar{1}0]$ direction is still parallel to the x direction and the unit cells are tilted about that axis by an angle of $\pm29^\circ$. This orientation was produced by the longitudinal rolling. The only effect of the second, transverse rolling was to reduce the angle of tilt (although it might have been smaller than in specimen 1 initially because of the lesser reduction of this specimen) and to change the distribution of the poles about the ideal orientation: there is less scatter in the angle of tilt but more scatter of the $[10\bar{1}0]$ direction about the x axis. In addition the texture has two very weak components corresponding to grains with the c axis parallel to the x and y directions respectively and $[10\bar{1}0]$ contained in the plane of the sheet.

Specimen 3, although it exhibits a highly textured character, is made up of more than one preferred orientation. The same orientation as above has survived the recrystallization treatment. $[10\bar{1}0]$ is parallel to the x axis;

the basal planes are rotated by 31°±2° about it, out of the plane of the sheet. The scatter of the [10$\bar{1}$0] direction about the x axis is quite considerable and it is not impossible that the orientation is actually double: in addition to the rotation about [10$\bar{1}$0] of the basal planes there is a small rotation of ±4° about a perpendicular to the plane of the sheet. A second series of high density areas corresponds to grains having their c axis along the x direction and the [10$\bar{1}$0] direction along the y axis. Finally there are two other sets of areas where poles are clustering, but to a lesser degree. However their interpretation is not unambiguous. In order to be able to draw definite conclusions a (0002) pole figure is required. The small number of grains having these orientations did not justify such an investigation. The corresponding areas of the pole figure can be interpreted as related to grains oriented with the c axis perpendicular and parallel to the plane of the sheet and the [10$\bar{1}$0] direction along the y axis and the sheet normal respectively. A partial survey of the central part of the pole figure using the back reflection method, seems to indicate the presence of a maximum at the center of the pole figure. This fact would support the preceding interpretation.

Table I which follows summarizes the texture of each specimen by giving its predominant orientations. Angles ω and χ of the sheet normal and the longitudinal direction with the c axis of each orientation are also listed. No attempt is made to explain these textures and to relate the recrystallization texture to the deformation texture from which it has been obtained. It shall only be noted that in the case of similar treatments, the results are in agreement with findings by Keeler and Geisler[24].

Specimen	μt	Orientations	ω	χ
1	.67	$[10\bar{1}0]$ parallel to Ox (L.D.) (0002) face tilted about Ox, 45° out of the xy plane	45°	90°
2	1.01	a. $[10\bar{1}0]$ parallel to Ox (L.D.) [0001] tilted 30° in the transverse direction	30°	90°
		b. [0001] parallel to Oy (T.D.) $[10\bar{1}0]$ parallel to Ox (L.D.)	90°	90°
		c. [0001] parallel to Ox [1010] parallel to Oy	90°	0
3	1.01	d. $[10\bar{1}0]$ parallel to Ox [0001] tilted 30° in the transverse direction	30°	90°
		e. [0001] parallel to Ox [1010] parallel to Oy	90°	0
		f. [0001] parallel to Oy $[10\bar{1}0]$ parallel to Oz	90°	90°

TABLE I

5. EXPERIMENTAL RESULTS

Each of the three specimens, prepared and examined for texture, was then mounted on the specimen holder and its resistivity and Hall coefficient measured between 4.2°K and room temperature as has been described in section 3. The results are presented below and are summarized in Table II.

5.1 Electrical Resistivity

The results of measurements of the electrical resistivity of the three specimens investigated are plotted on Fig. 23. Although the curves are very similar in shape and at a given temperature the resistivities of the three samples are not too different, the slopes of the linear portion of these curves differ from specimen to specimen. Before these differences can be attributed to anisotropy, it must be verified that they are not simply due to experimental errors. As seen earlier, whereas the value of the resistance is accurately known, there is a 4% uncertainty in the geometrical factor k_1 and hence the resistivities. This uncertainty does not affect much the low temperature part of the curve, but near room temperature a 4% change in the resistivity of specimen 1 would transform it to a value very close to the resistivity of specimen 2 at that temperature. A 3% decrease of the resistivities of specimen 1 and a 2% increase of the resistivities of specimen 2 makes these two curves coincide over almost the whole range of temperature. Furthermore, this common curve is much closer to a straight line and thus more likely correct, if the Gruneisen formula is assumed to hold. As far as specimen 3 is concerned, the uncertainty in k_1 is not sufficient to brings its resistivity curve in coincidence with the others. It can be noticed, however, that the slope of this curve is nearly

	Specimen	Dimensions (cm)	Resistivity ($\mu\Omega$cm)	$\rho_{295}/\rho_{4.2}$	ρ_{295}/ρ_{77}	Hall coefficient (m^3/C)	$R_{\parallel}$ & $R_{\perp}$ $\times 10^{11}$ m^3/C
1	4.2°K	ℓ: 12.72	1.80	26.9	7.95	$-6.9.10^{-11}$	Room temperature
	77.4	b: 3.86	6.10			$-2.63.10^{-11}$	$R_{\parallel} = 4.2$
	295	t: .0066	48.5			$-1.75.10^{-11}$	$R_{\perp} = -7.7$
2	4.2°K	ℓ: 12.08	1.56	28.6	7.65	$-4.65.10^{-11}$	77.4°K:
	77.4	b: 4.14	5.85			0	$R_{\parallel} = 2.63$
	295	t: .0093	44.7			$+1.20.10^{-11}$	$R_{\perp} = -7.9$
3	4.2°K	ℓ: 12.08	1.23	34.4	7.62	$-6.45.10^{-11}$	4.2°K:
	77.4	b: 4.14	5.60			$-2.75.10^{-11}$	$R_{\parallel} = -2.4$
	295	t: .0093	42.2			$-1.84.10^{-11}$	$R_{\perp} = -11.4$

TABLE II

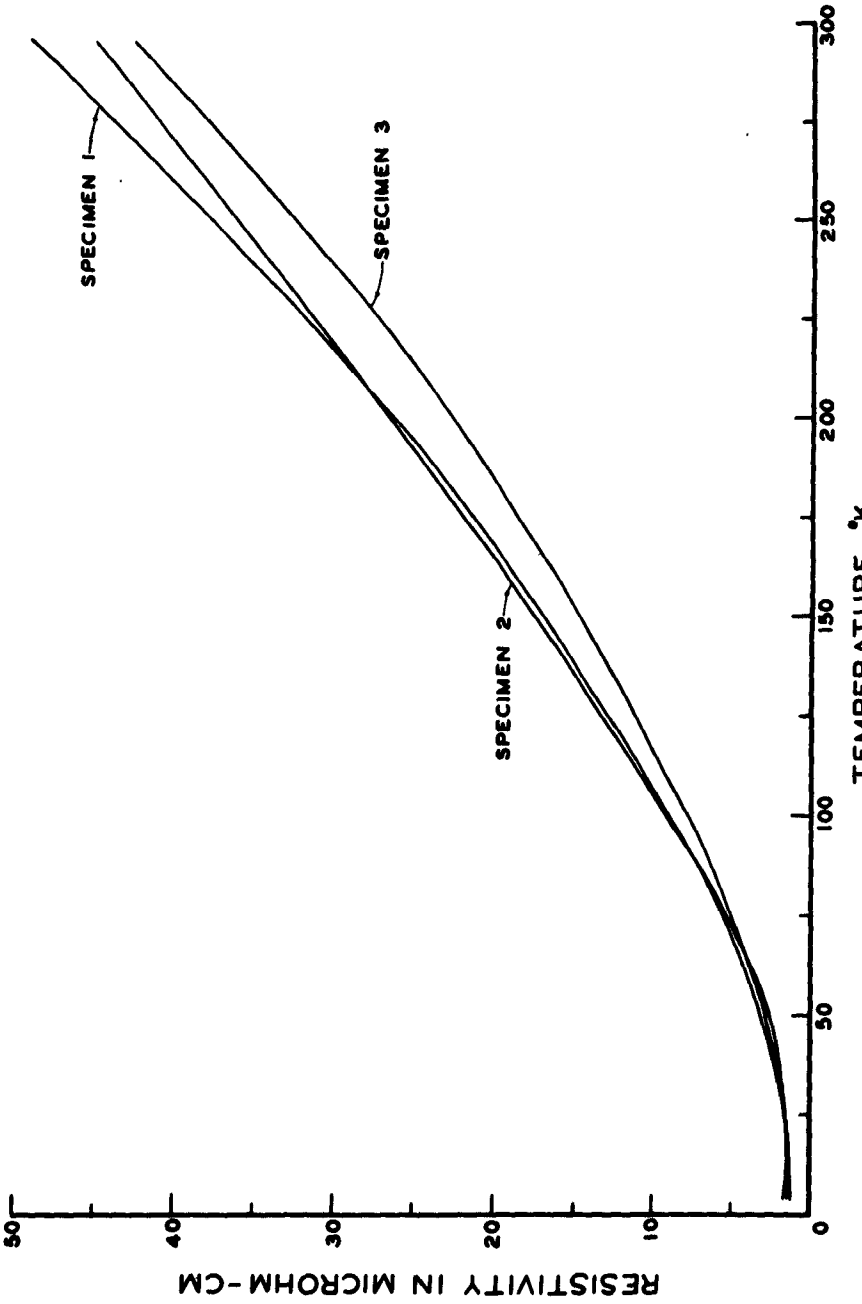

Fig. 23. Electrical resistivity versus temperature curves for three titanium specimens.

the same as the slope of the curve common to specimens 1 and 2: the two principal components $\rho_{\parallel}$ and $\rho_{\perp}$ of the resistivity tensor have a very similar temperature dependence.

Coming to the value of the residual resistance and the resistance ratios, an indication of the purity of the material, it is seen that the values obtained differ by more than 4%. The differences are significant (especially for the resistance ratios where the uncertainty in k_1 does not come in) and can be interpreted in terms of a difference in purity of the samples, in addition to the anisotropy effect. Specimen 1 might have suffered a slight contamination during its preparation. The better conducting properties of specimen 3 most likely have their origin in the annealing treatment which eliminated many lattice defects, unaffected by treatments at lower temperatures.

The values of resistivity obtained in this investigation are in good agreement with published data[6,25] and the spread in the values both at room temperature and 4.2°K seems to have been less extensive than has been reported previously. This arises probably from the fact that the samples were all made from the same piece of titanium.

5.2 Hall Coefficient

The variation with temperature of the Hall coefficient R_H for the three specimens is displayed in Fig. 24. Whereas two of the samples have very comparable Hall coefficient versus temperature cuves, specimen 2 shows a quite different behavior. Before making any further comments on these curves, it should be noted that it is meaningful to characterize

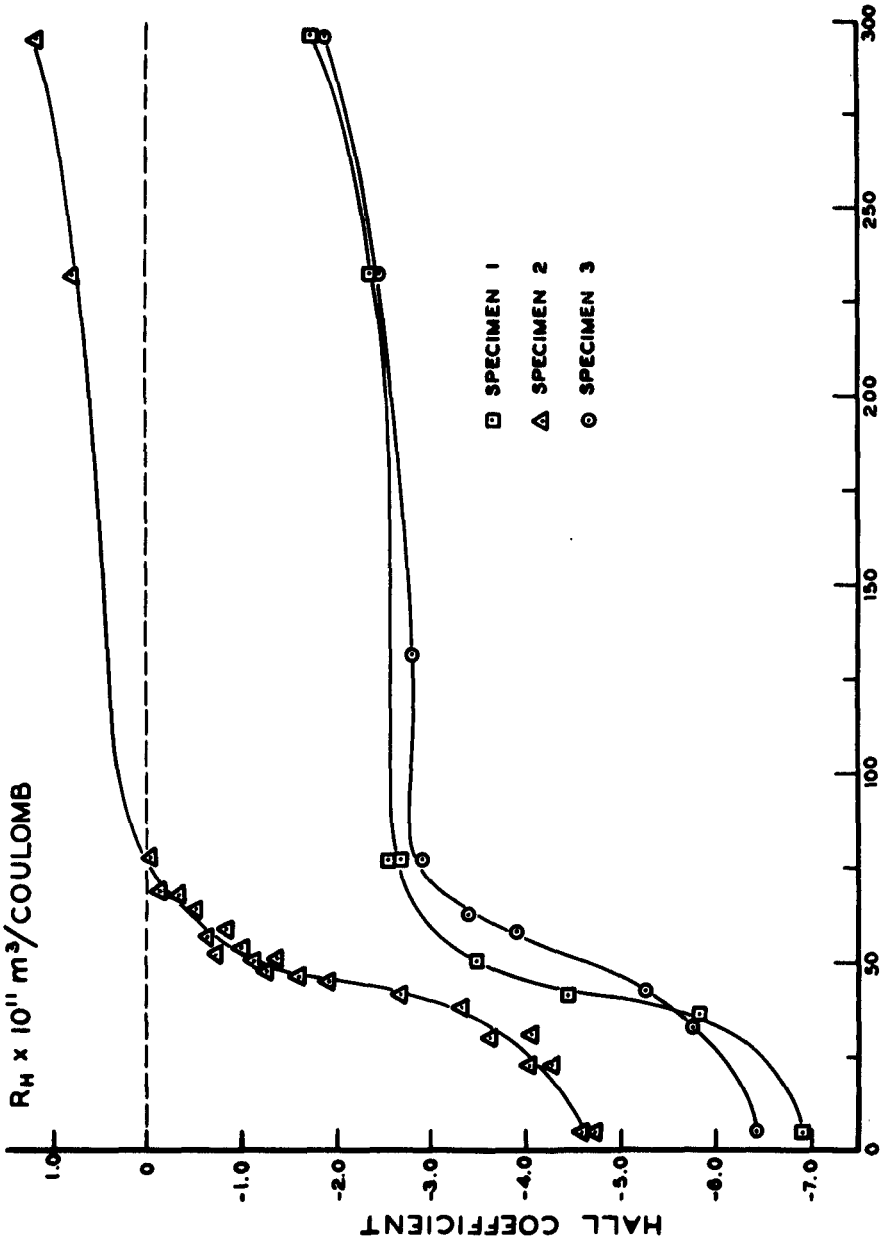

Fig. 24. Hall coefficient versus temperature curves for three titanium specimens.

the temperature dependence of R_H by a single curve only when R_H is independent of the magnetic field. Earlier investigations as well as the data shown in Fig. 25 clearly establish the proportionality of the Hall voltage with magnetic field. Therefore the Hall coefficient can be derived from measurements at any field strength and the observed discrepancies have to be attributed to some other cause.

The most striking feature in common to the three curves is their general form, very much reminiscent of the lattice specific heat curves. This suggests that the mechanism of scattering of the electrons by the lattice might be an important factor in determining R_H together with the electronic structure. In many cases the latter factor is more important and R_H varies little with temperature. For titanium at low temperatures the opposite situation might exist. Above 100°K a more usual behavior, with an almost constant Hall coefficient, is observed.

The major difference between specimen 2 and the others is the positive value of its Hall coefficient above 77°K. If the differences in Hall coefficient are attributed to anisotropy, this means that there must exist one or several crystallographic directions, in which the Hall coefficient is positive. In a detailed interpretation of the results, other factors like impurities will also have to be considered. The numbers themselves agree with results of other investigators: values in the same intervals are obtained at all temperatures. It has been attempted in this study to get a more detailed shape of the R_H versus T curves in order to make sure that their slope does not change sign above 77°K as one of Berlincourt's samples seemed to indicate (a difference in texture could account for this fact).

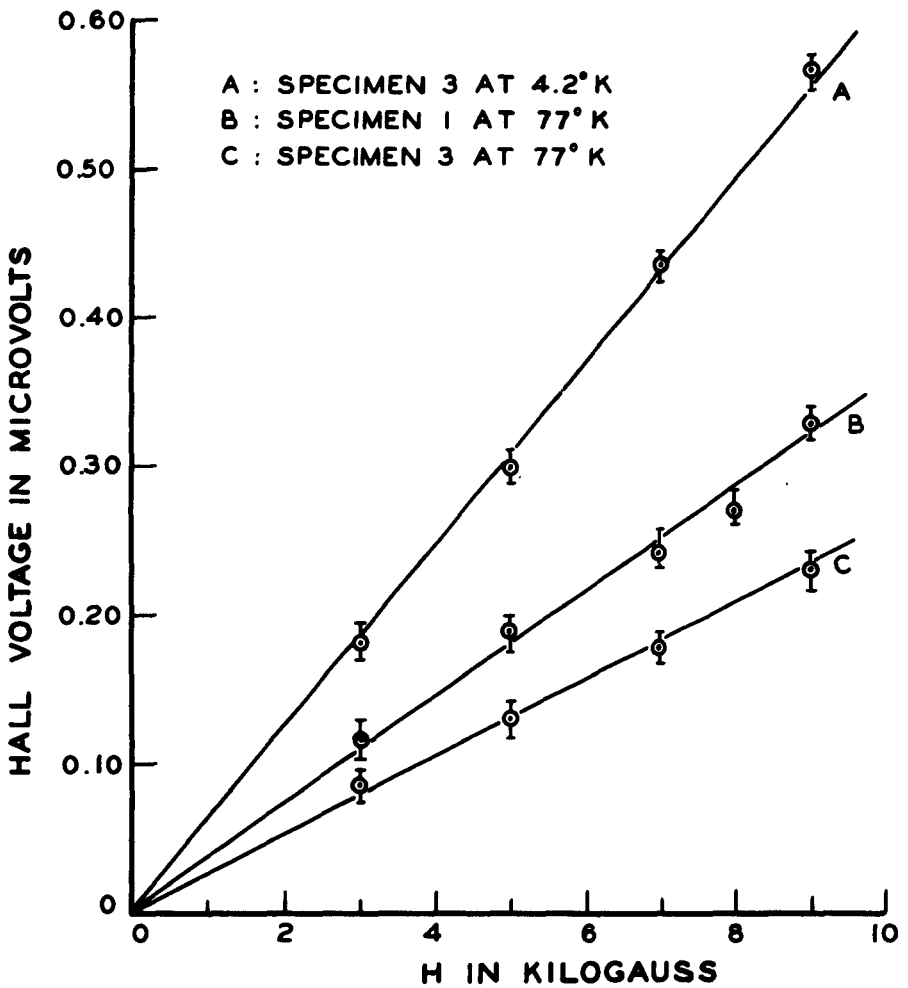

Fig. 25. Dependence of the Hall voltage on magnetic field strength.

6. DISCUSSION

The electrical properties of titanium measured in this study will now be discussed on the basis of the band theory of solids and the phenomenological theory of the Hall effect developed in section 2. Titanium has the electronic configuration $3d^2 4s^2$ and hence has four electrons beyond the argon shell. At $0^\circ K$, these electrons, which are responsible for the properties under consideration, occupy energy states in wave number or k-space up to W_F, the Fermi energy. The kinetic energy of the electrons, $W(\vec{k})$, is not a continuous function of $\vec{k}$. Discontinuities occur at certain sets of planes forming a polyhedron, the Brillouin zone. Since the electrical properties of solids are determined by electrons occupying energy states near the Fermi energy, they depend strongly on the relative configuration of the Fermi surface $W_F(\vec{k})$ and the Brillouin zone boundaries. In the reduced zone scheme, the Fermi surface consists of portions of surfaces belonging to different Brillouin zones and the contributions to the electrical properties from these various surfaces may be quite different (multi-band models). In the case of titanium, it could be attempted to explain the observed properties from a preconceived model of its Fermi surface, which could then be refined. The assumed band structure consists of two or three overlapping Fermi surfaces[17]: one (or two) 3d band(s) and a normal 4s band. Each of the bands associated with the different surfaces is assumed to be almost filled. In addition, an upper band, completely empty and separated from the others by an energy gap, is assumed to exist.

6.1 Electrical Resistivity

The electrical resistivity of titanium is particularly high in comparison to copper and even its immediate neighbors in the first transition series. This high value is in agreement with the small density of vacant states near the Fermi energy predicted by the proposed band structure. The variation of electrical resistance with temperature is expected to be linear for temperatures above the Debye temperature as long as there is no change in the band structure. Although the linearity is not clearly apparent in the plots of Fig. 24 because of the error in the factor k_1, a curve of the resistance ratio $R(T)/R(295^\circ)$ shows it much better. The departure from linearity in the direction of lower conductivities is explained by the presence of lattice defects introduced during the preparation of the specimens. A departure in the opposite direction, due to the increase of conducting states as electrons are thermally excited into the upper band, becomes important only at higher temperatures (above 200°C).

However, as noted earlier, experimental uncertainty is not sufficient to account for the different behavior of the three specimens. A difference in purity is most certainly a factor favoring such differences. Since no quantitative analysis is available, no definite conclusions are possible. However, it is not believed that the small amount of impurities present is the only factor. Another explanation takes into account the anisotropy of the Fermi surface in relation to the hexagonal symmetry. Conductivity is characterized by a tensor which has two independent components $\rho_\parallel$ and $\rho_\perp$. If in a single crystal the current

makes an angle χ with the hexagonal axis, the resistivity measured in that direction is[26]:

$$\rho(\chi) = \rho_{\parallel}\cos^2\chi + \rho_{\perp}\sin^2\chi$$

The resistivity of a polycrystalline sample is an average of the resistivities of all its grains:

$$\rho = \frac{\int_0^{\pi/2}\rho(\chi)\, n(\chi)\, d\chi}{\int_0^{\pi/2} n(\chi)\, d\chi}$$

in which $n(\chi)\, d\chi$ is the number of grains, the $\underline{c}$ axis of which makes an angle between $\pm\chi$ and $\pm(\chi + d\chi)$ with the direction of the current. This formula neglects grain boundary effects and is therefore not very realistic. Knowing $n(\chi)$, ρ can be calculated in terms of $\rho_{\parallel}$ and $\rho_{\perp}$ and conversely $\rho_{\parallel}$ and $\rho_{\perp}$ can be deduced from the resistivity of several textured specimens for which $n(\chi)$ is known from the pole figure. If the distribution of poles is sharply peaked about a small number of angles, $n(\chi)$ can be approximated by a set of delta functions and

$$\rho = n_1\rho(\chi_1) + n_2\rho(\chi_2) + \ldots$$

where n_1, n_2 .. are the fractions of grains having orientations χ_1, χ_2 .. respectively.

In specimens 1 and 2, only one orientation is predominant: $\chi = 90°$. The corresponding resistivities are $\rho_1 = \rho_{\perp}$ and $\rho_2 = \rho_{\perp}$. In specimen 3 two irientations are important: $\chi_1 = 90°$ and $\chi_2 = 0$ with $n_1 \simeq .7$ and $n_2 \simeq .3$. Then $\rho_3 = .3\,\rho_{\parallel} + .7\,\rho_{\perp}$. Plugging the room temperature values into these equations one obtains $\rho_{\parallel} = 35\,\mu\Omega\text{cm}$, $\rho_{\perp} = 47\,\mu\Omega\text{cm}$.

These results are not very meaningful because ρ_1, ρ_2, ρ_3 involve a large uncertainty and because the distribution functions $n(\chi)$ have been oversimplified. There are reasons to believe that $\rho_{\parallel}$ and $\rho_{\perp}$ are almost equal. Therefore reliable values can only be obtained by using single crystals and measuring in various directions on the same sample. The difficulty in the interpretation of the present results comes from the fact that several factors act simultaneously and not enough information about them is available. Experimental uncertainty furthermore reduces the chances of a detailed explanation.

If derivable from the experimental results, the values of $\rho_{\parallel}$ and $\rho_{\perp}$ could be used to deduce certain features of the Fermi surface in the a and c directions. In fact $\rho_{\parallel}$ and $\rho_{\perp}$ are given by the following expressions:

$$\frac{1}{\rho_{\parallel}} = \frac{e^2}{4\pi^3}\int_{F.S.} \tau(\vec{k}) \left(\frac{\partial W_F}{\partial k_3}\right)^2 \frac{dS}{|\mathrm{grad}_k W_F|} \quad ;$$

$$\frac{1}{\rho_{\perp}} = \frac{e^2}{4\pi^3}\int_{F.S.} \tau(\vec{k}) \left(\frac{\partial W_F}{\partial k_2}\right)^2 \frac{dS}{|\mathrm{grad}_k W_F|}$$

in which the integration is over the Fermi surface, $\tau(\vec{k})$ is the relaxation time and $W_F(\vec{k})$ the Fermi energy.

The use of these expressions in the hope of refining the picture of the Fermi surface requires accurate data. But even then the interpretation is delicate and not always unique. The fact that the Fermi surface overlaps or nearly overlaps the Brillouin zone in certain directions in k-space would account for a smaller resistivity in the corresponding directions of the real lattice.

6.2 Hall Coefficient

The Hall coefficient at a given temperature can be interpreted on the basis of several possible models. Titanium being a transition metal with two types of charge carriers, a two band model has to be chosen. The isotropic two band model gives the Hall coefficient as:

$$R_H = -\frac{1}{ec}\,\frac{\frac{\sigma_{01}^2}{n_1} - \frac{\sigma_{02}^2}{n_2} + \left(\frac{H}{ec}\right)^2 \frac{n_1 - n_2}{n_1^2 n_2^2}\,\sigma_{01}^2\,\sigma_{02}^2}{(\sigma_{01}+\sigma_{02})^2 + \left(\frac{H}{ec}\right)^2 \frac{(n_1 - n_2)^2}{n_1^2 n_2^2}\,\sigma_{01}^2\,\sigma_{02}^2}$$

In this expression σ_{01} is the conductivity of electrons of band 1 when $H = 0$, n_1 is their density of states near the Fermi energy; σ_{02}, n_2 are the corresponding values of band 2. On the same model the conductivities are given by:

$$\sigma = \sigma_{01} + \sigma_{02} = e^2\left(\frac{n_1 \tau_1}{m_1} + \frac{n_2 \tau_2}{m_2}\right)$$

There are thus six unknown parameters and only two experimental values to determine them. It is therefore not surprising that almost any experimental curve $R_H(T)$ or $\rho(T)$ can be fitted by an appropriate choice of these parameters and their temperature dependence. In order to determine them uniquely, other properties have to be measured in terms of the same set of parameters, which should then be able to predict additional properties of the material. However it often turns out that the same set of parameters is not able to describe several properties simultaneously (for example Hall effect and magnetoresistance). The procedure is therefore

mere curve fitting and has not much in common with a realistic picture of the electronic structure. In addition this model does not allow to predict different values of R_H for different specimens of the same material.

Impurities have often been held responsible for the scatter of the experimental data. In the present case, however, the three specimens had very comparable purity because they were made out of the same piece of titanium and great care was taken in the preparation of the samples. Furthermore, the fact that specimens 2 and 3, actually the same piece of material, gave drastically different Hall constants (even the sign of R_H changed) just by heat treatment, seems to rule out the influence of impurities as predominant cause of differences in R_H. However, other experiments and theory show that impurities affect the Hall coefficient much more strongly than other properties like resistivity. The effect of impurities cannot be completely neglected in a detailed discussion.

Similarly it is not very likely that a size effect could explain the differences observed. In copper, where systematic studies of such an effect have been made[27], R_H was found independent of thickness provided t was larger than the electronic mean free path ($t > 0.1$ mm). In this study t was in this critical range. However the mean free path in titanium is expected much shorter than in very pure copper. In addition specimens 1 and 3 had different thicknesses but similar Hall coefficients. Although a size effect cannot be completely put aside, it is not sufficient to explain the experimental results. At any rate such an effect is not well understood and would be difficult to be evaluated quantitatively.

On the other hand, it is possible to obtain a consistent interpreta-

tion of the results of the measurements by assuming a dependence of the Hall coefficient on crystallographic direction. In each grain the Hall coefficient becomes then a function of the angle ω between the magnetic field and the hexagonal axis:

$$R_H(\omega) = R_{\parallel} \cos^2\omega + R_{\perp} \sin^2\omega$$

It varies from $R_{\parallel}$ to $R_{\perp}$ in a continuous fashion and, since both positive and negative values of R_H have been measured, one of these two coefficients is negative and the other positive. In the case of a polycrystalline sample the measured Hall coefficient is a weighted average of the contributions from the different grains depending on their orientation with respect to the magnetic field:

$$R_H = \frac{\int_0^{2\pi} d\phi \int_0^{\pi} n(\omega,\phi)\, R_H(\omega)\, \sin\omega\, d\omega}{\int_0^{2\pi} d\phi \int_0^{\pi} n(\omega,\phi)\, \sin\omega\, d\omega}$$

In this formula $n(\omega,\phi)$ is the number of grains per unit solid angle the hexagonal axis of which has polar angles ω and ϕ in the xyz system of coordinates. Proceeding as in 6.1, we replace each textured specimen by its ideal orientation in order to get order of magnitude estimates of $R_{\parallel}$ and $R_{\perp}$.

Specimen 1: $R_H^1 = \frac{1}{2}(R_{\parallel} + R_{\perp})$ $(\omega = 45°)$

Specimen 2: $R_H^2 = \frac{1}{4}(3R_{\parallel} + R_{\perp})$ $(\omega = 30°)$

Specimen 3: $R_H^3 = .30\, R_H(90°) + .70\, R_H(30°) =$

$$.48R_{\perp} + .52R_{\parallel}$$

At room temperature the values of R_H^1 and R_H^2 lead to $R_{\parallel} = +4.2$ and

$R_\perp$ = -7.7 in units of 10^{-11} m^3/coulomb. Substituting these values into R_H^3 one gets R_H^3 = -1.5 instead of the measured value of -1.84. At liquid nitrogen temperature, one obtains similarly $R_\parallel$ = +2.63 and $R_\perp$ = -7.9 and a calculated value for R_H^3 of -2.4 instead of -2.75. At liquid helium temperature, the corresponding values are: $R_\parallel$ = -2.4, $R_\perp$ = -11.4 and R_H^3 = -6.75 instead of -6.45, the observed value.

At least qualitatively the results are consistent. For specimen 3 one of the components of the texture favors a positive Hall coefficient and the other a strongly negative value; the overall effect is a negative R_H^3. The magnitudes of $R_\parallel$ and $R_\perp$ given above are more questionable, in view of the uncertainty in R_H and especially the crude assimilation of a textured sample to a perfect single crystal. Calculations with more detailed expressions for $n(\omega, \phi)$, as can be constructed from the pole figures, would not produce much more reliable numbers, the effect of grain boundary scattering and all lattice imperfections being neglected. However, it is believed that the difference in sign of the two coefficients is significant. It should finally be noted that the values of $R_\parallel$ and $R_\perp$ given above allow to account for the spectrum of Hall coefficient values published before.

Before commenting on the consequences of opposite signs of the two principal Hall coefficients, a brief remark will be made on the temperature dependence of R_H. As noted earlier and as can be seen from the results just given, R_H^1, R_H^2, R_H^3 as well as $R_\parallel$ and $R_\perp$ have very much the same type of temperature variation, analogous to lattice specific heat curves, although the extent of this variation may depend on crystallographic

direction. R_H could therefore depend on the mechanism of scattering: at low temperature impurity scattering is predominant, whereas near room temperature lattice scattering is more important. The two mechanisms may very well lead to different values of the relaxation time and hence the Hall coefficient. However if this were true, a similar effect should be observed for all metals. A better explanation may therefore be found in very sensitive overlap conditions of the different sheets of the Fermi surface.

A tempting explanation of the difference in sign of $R_{\parallel}$ and $R_{\perp}$ involves very sensitive overlap conditions of the energy surfaces among themselves and with the Brillouin zone, which depend on the direction in k-space. However, in order to relate $R_{\parallel}$ and $R_{\perp}$ to the constant energy surfaces, a detailed model of the transport problem has to be developed, taking into account the anisotropy of the Fermi surface, the anisotropy of the scattering, impurity effects, etc. It is not possible to rely only on intuitive arguments or qualitative reasoning. The Hall coefficient depends much more on the detailed shape of the Fermi surface than resistivity, for instance, and in each of the components of the galvanomagnetic tensor, contributions from all parts of the Fermi surface have to be considered. A theoretical formula taking these factors into account can be derived from the Boltzmann transport equation by assuming the existance of a relaxation time $\tau(\vec{k})$. In the first order in the magnetic field, the following formula is obtained for the Hall coefficient[28]:

$$R_H(\vec{k}) = \frac{2}{eN_xN_y} \int_{F.S.} \left[\left(\frac{\partial W}{\partial k_y} \right)^2 \frac{\partial^2 W}{\partial k_x^2} - \frac{\partial W}{\partial k_x} \frac{\partial W}{\partial k_y} \frac{\partial^2 W}{\partial k_x \partial k_y} \right] \tau^2(k) \frac{dS}{|\mathrm{grad}_k W|} \qquad (a)$$

In this formula $W(\vec{k})$ is the Fermi energy. The integration is over the Fermi surface. Current, magnetic field and Hall field are directed as in Fig. 3a and

$$N_x = 2\int_{F.S.} \left(\frac{\partial W}{\partial k_x}\right)^2 \tau(\vec{k}) \left|\frac{dS}{\text{grad}_k W}\right|$$

$$N_y = 2\int_{F.S.} \left(\frac{\partial W}{\partial k_y}\right)^2 \tau(\vec{k}) \left|\frac{dS}{\text{grad}_k W}\right|$$

If the crystal is oriented with its principal directions along the xyz coordinates axes, the expression for the Hall coefficient reduces to:

$$R_H(\vec{k}) = \frac{2}{eN_xN_y} \int_{F.S.} \left(\frac{\partial W}{\partial k_y}\right)^2 \frac{\partial^2 W}{\partial k_x^2} \tau^2(\vec{k}) \left|\frac{dS}{\text{grad}_k W}\right| \qquad (b)$$

N_x and N_y are respectively proportional to σ_x and σ_y, the conductivities in the x and y directions. Formula (b) can be used to calculate $R_{\parallel}$ and $R_{\perp}$ if the functional form of $W(\vec{k})$, the equation of the Fermi surface, is given. The sign of R_H depends therefore on $\partial^2 W/\partial k_x^2$, a quantity which is proportional to the reciprocal effective mass in the direction of the current, which was not obvious a priori. R_H is, however, a weighted average of this quantity over the entire Fermi surface. Negative and positive contributions to R_H can be distinguished by considering separately regions of the Fermi surface where the curvature is positive and negative. R_H, which is a measure of the difference of carriers having electron-like properties (positive curvature) and the number having hole-like properties (negative curvature), is then given by[29]:

$$R_H = \frac{h^3}{2ec}\left\{\int_{F.S.} dp_z \left[S_e(W_F, P_z) - S_h(W_F, P_z)\right]\right\}^{-1} \qquad (c)$$

where $P_z = \hbar k_z$ is the component of the electron momentum in the direction of the magnetic field, S_e and S_h are closed areas formed by the intersection of the Fermi surface with a plane perpendicular to k_z. Electron-like properties are associated with areas which have states having energies less than W_F, hole-like properties with areas which have states of energy greater than W_F. In formulas (b) and (c) it is apparent that the Hall constant depends on the detailed shape of the Fermi surface. A vague model is not sufficient to predict, even in a semi-quantitative way, the sign of R_H and certainly not its magnitude. In the case of titanium, where the Fermi surface is multiply connected, there is little hope to deduce it from the knowledge of $R_H(\vec{k})$ and $\rho(\vec{k})$ alone.

If the Fermi surface is taken as an ellipsoid of revolution, $R_{\parallel}$ and $R_{\perp}$ can be calculated in terms of its axial lengths, which in turn can be related to the carrier density and their effective mass. To do this, equation (b) together with similar expressions for the conductivity, has to be used. However, this model is not very realistic since it does not explain positive values of R_H (for an ellipsoid, the curvature is always positive and hence R_H negative). Two techniques can be used to improve the estimate. Assuming a simply connected Fermi surface, its shape might be determined by solving the integral equation (a) where $R_H(\vec{k})$ has been determined experimentally for all orientations of $\vec{k}$. The second solution considers the Fermi surface as made up of two interpenetrating sheets corresponding one to electrons, the other to holes. If ellipsoids of the same orientation are taken as first approximation, H. Jones[30] has shown that the Hall coefficient could be written:

$$R_H = \frac{\frac{c}{e}\left\{\left[\frac{\sigma_x^{(+)}\sigma_y^{(-)}}{n^{(-)}} - \frac{\sigma_x^{(+)}\sigma_y^{(+)}}{n^{(+)}}\right]\frac{1}{\sigma_x\sigma_y} + \frac{\sigma_x^{(-)}\sigma_x^{(+)}\sigma_y^{(-)}\sigma_y^{(+)}}{\left[n^{(-)}n^{(+)}\right]^2}\frac{\left[n^{(-)}-n^{(+)}\right]^2}{\sigma_x\sigma_y}\left(\frac{eH}{c}\right)^2\right\}}{1 + \frac{\sigma_x^{(-)}\sigma_y^{(+)}\sigma_y^{(-)}\sigma_y^{(+)}}{\left[n^{(-)}n^{(+)}\right]^2}\frac{\left[n^{(-)}-n^{(+)}\right]^2}{\sigma_x\sigma_y}\left(\frac{eH}{c}\right)^2} \qquad (d)$$

$\sigma_x(-)$ is the contribution of electrons to the conductivity in the x direction. $\sigma_x(+)$ is the contribution of holes to the conductivity in the x direction. $\sigma_x = \sigma_x(-) + \sigma_x(+)$

$n^{(-)}$ and $n^{(+)}$ are the density of electrons and holes near the Fermi surface in k-space.

The partial conductivities are expressible in terms of the axial lengths of the corresponding ellipsoid. The experiment yields four values: $R_{\parallel}$, $R_{\perp}$, $\rho_{\parallel}$ and $\rho_{\perp}$. However, there are six unknowns. So, even with this imperfect model, there is no unique determination of the energy surfaces in the solid. If, furthermore, the assumption of an ellipsoidal Fermi surface is not made, many shapes can be found for the Fermi surface, which account for the observed Hall coefficients. Therefore, before any quantitative interpretation of the Hall measurements can be attempted, a fairly detailed model of the Fermi surface of titanium must be worked out. Such a model is not available yet, but should be obtained in the next few years by means of the topological methods. These more direct methods have replaced Hall measurements in the systematic investigation of Fermi surface topology.

It should be noted that, if the functional relationship $W(\vec{k})$, i.e., the equation of the Fermi surface, possesses the point group symmetry of

the crystal, formulas (a) and (d) give the same dependence of Hall coefficient on orientation as the phenomenological theory presented in section 2. In many cases this fact is not obvious by just looking at the integrals, but can be checked in each case by carrying out the calculations, using a specific function $W(\vec{k})$ having the proper symmetry. The difference between the physical and the phenomenological approaches arises from the fact that one expresses everything in terms of conductivities and the other in terms of resistivities. The results however are in agreement.

As far as the present study is concerned, the previous remarks will justify the fact that no conclusions are drawn from the relative signs and magnitudes of $R_{\parallel}$ and $R_{\perp}$. Nevertheless, there is little doubt that the positive sign of $R_{\parallel}$ is associated with a region of the Fermi surface very close to the Brillouin zone boundary, where the curvature is negative. However, it is not obvious in what directions in k-space this situation occurs. The hypothesis of an overlap at the (0002) faces of the Brillouin zone suggested by the Jones stress theory may not be the only possible explanation.

7. CONCLUSION

The investigation of the Hall coefficient of three specimens of iodide titanium from liquid helium to room temperatures has shown a strong dependence of this coefficient on temperature, impurity content, and preferred orientation. Although, at present, no general model can explain quantitatively all the observations, several factors can be considered. It is shown that impurities, size effects, changes in the scattering

mechanism and a dependence of Hall coefficient on crystallographic direction can account, at least in part, for the experimental results. Even if all these factors may play a certain role in the value of the Hall constant, the results of this investigation as well as of earlier work can factually be interpreted by considering only the orientation effect. The anisotropy of the hexagonal symmetry causes different values of R_H in different directions. A positive value is obtained when the magnetic field is directed along the c axis and a negative value occurs when it lies in the basal plane.

The fact that no definite conclusions are drawn from these findings, is due to the large number of unknown parameters that appear in the theoretical formulas derived from the transport equation. These parameters can be estimated from other properties or assumed by the model. Then some qualitative features of the Fermi surface could, in principle, be deduced from the Hall data. However it seems easier to work in the opposite direction and determine first, by experiment, values of those parameters and use topological methods to construct a model of the Fermi surface. The assumed electronic structure can then be tested by Hall measurements. This procedure is more satisfactory than just a fitting of the data by assuming a fairly arbitrary model, even if this model leads to not unreasonable results. In both cases the interpretation of the data may not be unique.

Although the information gained by Hall measurements is not complete and does not allow an overall picture of the electronic structure, such measurements are of high interest, especially if carried out with

single crystals. In the case of titanium the temperature range from 300 to 1100°K should also be reinvestigated. Such measurements would provide more accurate and more reliable values of the galvanomagnetic coefficients. By combining these values with other results, a more detailed model of the Fermi surface may be derived and the Hall effect data may be useful to decide between several possible models. In the case of copper, a similar procedure has been successfully carried out[29]. Eventually it may become possible to use the same model together with a consistent set of formulas to give correctly all the major electronic properties: specific heat, magnetic susceptibility, resistivity, galvanomagnetic and thermomagnetic effects, refractive index... In the case of titanium, where many of these properties depend on orientation, this situation is far from being attained.

REFERENCES

1. E. H. Hall, Am. Journal of Math. (1879), vol. 2, p. 287.
2. S. Foner, Phys. Rev. (1957), vol. 107, pp. 1513-1516.
3. G. W. Scovil, J. Appl. Phys. (1953), vol. 24, pp. 226-227.
4. G. W. Scovil, J. Appl. Phys. (1956), vol. 27, pp. 1196-1198.
5. S. Foner, Phys. Rev. (1953), vol. 91, p. 447.
6. T. G. Berlincourt, Phys. Rev. (1959), vol. 114, pp. 969-977.
7. A. J. Dekker, Solid State Physics (Prentice Hall, Inc., 1957), pp. 301-302 and 326-328.
8. J. P. Jan, Solid State Physics, Advances in Research and Applications (Academic Press Inc., New York, 1957), vol. 5, pp. 1-96.
9. M. Kohler, Ann. Physik (1934), vol. 20, pp. 878-890.
10. T. Okada, Mem. Fac. Sci. Kyusyu Univ. (1955), vol. B 1, pp. 157-168.
11. E. H. Hall, Phys. Rev. (1925), vol. 26, pp. 820-840.
12. F. J. Darnell, Trans. Met. Soc. AIME (1958), vol. 212, p. 356.
    R. J. Wasilewski, Trans. Met. Soc. AIME (1962), vol. 224, pp. 5-8.
13. H. Fritzsche, Methods of Experimental Physics - Solid State Physics (Academic Press, New York, 1959), vol. 6B, pp. 145-155.
14. S. Timoshenko, Theory of Plates and Shells (McGraw-Hill Book Co., 1940) pp. 199-232.
15. H. D. Baker, E. A. Ryder and N. H. Baker, Temperature Measurement in Engineering (J. Wiley & Sons, Inc., New York, 1961), vol. II, pp. 5-33.
16. J. M. Denney, Ph.D. Thesis (1954), California Institute of Technology, pp. 66-68.
17. R. H. Willens, Ph.D. Thesis (1961), California Institute of Technology, p. 88 and pp. 100-102.

18. B. D. Cullity, Elements of X-ray Diffraction (Addison-Wesley Publishing Co., 1959), pp. 272-295.

19. R. Smoluckowski and R. W. Turner, Rev. Sci. Instr. (1949), vol. 20, pp. 173-174.

20. B. F. Decker, E. T. Asp and D. Harker, J. Appl. Phys. (1948), vol. 19, pp. 388-392.

21. J. B. Newkirk and L. Bruce, G. E. Research Lab. Rept. No. 57-RL-1810 (1957), pp. 1-17.

22. B. F. Decker, E. T. Asp and D. Harker, J. Appl. Phys. (1948), vol. 19, pp. 391-392.

23. M. Schwartz, J. Appl. Phys. (1955), vol. 26, pp. 1507-1513.

24. J. H. Keeler and A. H. Geisler, Trans. AIME (1956), vol. 206, pp. 80-90.

25. J. L. Wyatt, J. Metals (1953), vol. 5, pp. 903-905.

26. A. H. Wilson, The Theory of Metals (Cambridge University Press, 1958), pp. 196-197.

27. T. G. Berlincourt, Phys. Rev. (1958), vol. 112, pp. 381-387.

28. N. F. Mott and H. Jones, The Theory of Properties of Metals and Alloys (Dover Publications, Inc., 1936 & 1958), pp. 280-285.

29. J. E. Kuntzler and J. R. Klauder, Phil. Mag. (1961), vol. 6, 8th Series, pp. 1045-1051.

30. H. Jones, Proc. Roy. Soc. (1936), vol. A 155, pp. 653-660.

DISTRIBUTION LIST

A

AGENCY	NUMBER OF COPIES
Air Force Office of Scientific Research ATTN: Solid State Sciences Division Washington 25, D.C.	3
Air Force Office of Scientific Research ATTN: Technical Library (SRGL) Washington 25, D. C.	2
ASTIA (TIPCR) Arlington Hall Station Arlington 12, Va.	10
ARDC (RDRS) Andrews AFB Washington 25, D.C.	1
EOAFRD ARDC 47 Cantersteen Brussels, Belgium	1
HQ USAF (AFDRT) Washington 25, D.C.	1
ARL (Technical Library) Bldg. 450 Wright-Patterson AFB, Ohio	1
WADD (WWAD) Wright-Patterson AFB, Ohio	1
WADD (Metals & Ceramics Lab) Materials Central Wright-Patterson AFB, Ohio	1
WADD (Physics Lab) Materials Central Wright-Patterson AFB, Ohio	1
WADD (Materials Information Branch) Materials Central Wright-Patterson AFB, Ohio	1
Institute of Technology (AU) Library MCLI-LIB, Bldg. 125, Area B Wright-Patterson AFB, Ohio	1

AGENCY	NUMBER OF COPIES
ARL (Metallurgy) AFRD Wright-Patterson AFB, Ohio	1
ARL (Physics, Solid State) AFRD Wright-Patterson AFB, Ohio	1
AFOSR (SRLTL) Holloman AFB, New Mexico	1
AFCRL (CRRELA) Laurence G. Hanscom Field, Bedford, Mass	1
AFFTC (FTCTL) Edwards AFB, California	1
AEDC (AEOIM) Arnold Air Force Station, Tennessee	1
AFSWC (SWOI) Kirtland AFB, New Mexico	1
Commander Army Rocket & Guided Missile Agency ATTN: ORDXR-OTL Redstone Arsenal, Alabama	2
Office of the Chief of Research and Development Department of the Army ATTN: Scientific Information Washington 25, D. C.	1
Army Research Office (Durham) ATTN: CRD-AA-IP Box CM, Duke Station Durham, North Carolina	1
Commanding Officer Ordnance Materials Research Office (ATTN: PS&C Div.) Watertown Arsenal Watertown 72, Massachusetts	1
Commanding Officer Watertown Arsenal ATTN: Watertown Arsenal Labs, Tech Reports Section Watertown 72, Massachusetts	1
Commander Signal Corps Engineering Laboratory ATTN: SIGFM/EL-RPO Fort Monmouth, New Jersey	1

AGENCY	NUMBER OF COPIES
Director US Naval Research Laboratory ATTN: Library Washington 25, D.C.	1
Department of the Navy Office of Naval Research ATTN: Code 423 ATTN: Code 421 Washington 25, D.C.	2
Officer in Charge Office of Naval Research Navy No. 100 Fleet Post Office New York, New York	1
Commanding Officer Naval Radiological Defense Laboratory San Francisco Naval Shipyard San Francisco 24, California	1
Dr. D. F. Bleil Associate Technical Director for Research US Naval Ordnance Lab White Oak, Silver Spring, Maryland	1
National Aeronautics & Space Agency ATTN: Library 1520 H St., N. W. Washington 25, D.C.	1
Ames Research Center (NASA) ATTN: Tech Library Moffett Field, California	1
High Speed Flight Station (NASA) ATTN: Tech Library Edwards AFB, California	1
Langley Research Center (NASA) ATTN: Tech Library Langley AFB, Virginia	1
Lewis Research Center (NASA) ATTN: Tech Library 21000 Brookpark Road Cleveland 35, Ohio	1
Wallops Station (NASA) ATTN: Tech Library Wallops Island, Virginia	1

AGENCY	NUMBER OF COPIES
Division of Research US Atomic Energy Commission Division Office Washington 25, D.C.	1
US Atomic Energy Commission Library Branch Tech Information Div., ORE P.O. Box No. E Oak Ridge, Tennessee	1
Major John Radcliffe ANP Office US Atomic Energy Commission Washington 25, D.C.	1
Oak Ridge National Laboratory ATTN: Central Files Post Office Box P Oak Ridge, Tennessee	1
Brookhaven National Laboratory ATTN: Research Laboratory Upton, Long Island, New York	1
Argonne National Laboratory ATTN: Librarian 9700 South Cass Avenue Argonne, Illinois	1
Document Custodian Los Alamos Scientific Laboratory P.O. Box 1663 Los Alamos, New Mexico	1
Ames Laboratory Iowa State College P.O. Box 14A, Station A Ames, Iowa	1
Knolls Atomic Power Laboratory ATTN: Document Librarian P.O. Box 1072 Schenectady, New York	1
National Science Foundation 1901 Constitution Avenue, N.W. Washington 25, D.C.	1
National Bureau of Standards Library Room 203, Northwest Building Washington 25, D.C.	1

AGENCY	NUMBER OF COPIES
Director Office of Technical Services Department of Commerce Technical Reports Branch Washington 25, D.C.	1
Chairman Canadian Joint Staff (DRB/DSIS) 2450 Massachusetts Avenue, N.W. Washington, D.C.	1
Defense Research Member Canadian Joint Staff ATTN: Mr. H. C. Oatway Director of Engineering Research Defense Research Board Ottawa, Canada	1
Institute of the Aeronautical Sciences ATTN: Librarian 2 East 64th Street New York 21, New York	1
RAND Corporation 1700 Main Street Santa Monica, California	2
Eastman Kodak Camera Works ATTN: W. L. McKusick Engineering Library Rochester 4, New York	1
Autonetics Division North American Aviation, Inc. ATTN: Technical Library Dept. 3040-1, Bldg. 2 9150 E. Imperial Highway Downey, California	1
Dr. David S. Lieberman Department of Mining & Metallurgy 205 Metallurgy Laboratory University of Illinois Urbana, Illinois	1
Engineering Library ATTN: Mr. Robert E. Fridoten Republic Aviation Corporation Farmingdale, Long Island, New York	1

AGENCY	NUMBER OF COPIES
R. C. Miltimore Sales Service Manager Industrial Division The J. M. Ney Company Hartford 1, Connecticut	1